Parameterized lattice strain models for REE partitioning between amphibole and silicate melt

KEI SHIMIZU^{1,*}, YAN LIANG¹, CHENGUANG SUN², COLIN R.M. JACKSON³, AND ALBERTO E. SAAL¹

¹Department of Earth, Environmental, and Planetary Sciences, Brown University, Providence, Rhode Island 02912, U.S.A.

²Department of Earth Science, Rice University, Texas 77005, U.S.A.

³Smithsonian Institution, Washington, D.C. 20013, U.S.A.

ABSTRACT

The distribution of rare earth elements (REEs) between amphibole and silicate melt is important for understanding a wide variety of igneous and metamorphic processes in the lithosphere. In this study, we used published experimental REE and Y partitioning data between amphibole and silicate melt, the lattice strain model, and nonlinear least-squares regression method to parameterize key partitioning parameters in the lattice strain model $(D_0, r_0, \text{ and } E)$ as a function of pressure, temperature, and both amphibole and melt compositions. Two models, which give nearly identical results, are obtained in this study. In the first model, D₀ depends on temperature and amphibole composition: it positively correlates with Ti content and negative correlates with temperature and Mg, Na, and K contents in the amphibole. In the second model, D_0 depends solely on the melt composition: it positively correlates with Si content and negatively correlates with Ti and Ca contents in the melt. In both the mineral and melt composition models, r₀ negatively correlates with the ferromagnesian content in the M4 site of the amphibole, and E is a constant. The very similar coefficients in the equations for r_0 and best-fit values for E in the two models allow us to connect the two models through amphibole-melt phase equilibria. An application of our model to amphiboles in mantle xenoliths shows that observed major element compositional variations in amphibole alone can give rise to order of magnitude variations in amphibole-melt REE partition coefficients. Together with experimental data simulating fractional crystallization of arc magmas, out models suggest that: (1) REE partition coefficients between amphibole and melt can vary by an order of magnitude during arc magma crystallization due to variation in the temperature and composition of the amphibole and melt, and that (2) amphibole fractional crystallization plays a key role in depleting the middle REEs relative to heavy REEs and light REEs in arc magmas.

Keywords: REE and Y partition coefficients, amphibole, amphibole melting in the mantle, amphibole fractional crystallization

Introduction

Amphibole is ubiquitous in the Earth's lithosphere, occurring in a wide variety of igneous and metamorphic rocks. As an inosilicate, amphibole has three main structural sites (A, M4, and M1–M3) that can accommodate cations of a range of size and charge. The general chemical formula of amphiboles may be described by the expression

where A = Na, K, or vacant (\square) in A site; B = Ca, Na, Mn, Fe^{2+} , Mg in M4 site; $C = Fe^{2+}$, Fe^{3+} , Mg, Al, Mn, Ti, Cr in M1, M2, and M3 sites; T = Si, Al in tetrahedral site (Hawthorne 1983). The smaller M1-M3 sites are in sixfold coordination, while the larger M4 site is in eightfold coordination. The latter can accommodate larger cations such as the trivalent rare earth elements (REE) and Y [ionic radii 0.977-1.16 Å, eightfold coordination, Shannon (1976)], while the smaller M1-M3 sites can accommodate smaller

cations such as high field strength elements.

The subject of the present study is REE partitioning between amphibole and silicate melt, which is important to understand the generation and differentiation of hydrous magmas. According to the lattice strain model (Blundy and Wood 1994; Brice 1975; Wood and Blundy 1997), the partition coefficients of trivalent REEs between amphibole and silicate melt vary systematically with their ionic radii:

$$D_{j}^{\text{amph-melt}} = D_{0} \exp \left[-\frac{4\pi E N_{A}}{RT} \left(\frac{r_{0}}{2} (r_{0} - r_{j})^{2} - \frac{1}{3} (r_{0} - r_{j})^{3} \right) \right]$$
(1)

where D_0 is the amphibole-melt partition coefficient for the strain-free substitution; r_0 is the radius of a hypothetical cation that substitutes into the site with zero strain; r_j is the ionic radius of the element of interest; E is the effective Young's modulus for the lattice site; N_A is Avogadro's number; $R = 8.3145 \text{ J/(mol \cdot K)}$] is the gas constant; and T is temperature in Kelvin. The lattice strain parameters (D_0, r_0, E) are, in general, a function of pressure (P), temperature (T), and composition (X).

Amphibole-melt REE partition coefficients have been shown to negatively correlate with *T* (Green and Pearson 1985; Klein et al. 1997; Nandedkar et al. 2016; Nicholls and Harris 1980) and *P*

^{*} Present address: Department of Terrestrial Magnetism, Carnegie Institution of Washington, 5241 Broad Branch Road NW, Washington, D.C. 20015, U.S.A. E-mail: kshimizu@carnegiescience.edu

(Adam and Green 1994, 2003; Dalpé and Baker 2000; Green and Pearson 1985), and positively correlate with the degree of melt polymerization (Brophy 2008; Green and Pearson 1985; Klein et al. 1997; Nandedkar et al. 2016; Nicholls and Harris 1980; Tiepolo et al. 2000, 2007). The effect of amphibole crystal chemistry on amphibole-melt REE partition coefficients has also been observed in previous studies. For example, greater occupancy of the A site by Na and K were shown to decrease the partition coefficients, presumably suggesting substitution of REEs in place of Na and Ca in the M4 site charge compensated by a vacancy in the A site (e.g., $Ca_{M4}^{2+}K_A^{+1} \leftrightarrow REE_{M4}^{3+}\square_A$) (Brenan et al. 1995; Green and Pearson 1985; Nicholls and Harris 1980). Also, amphibole-melt REE partition coefficients have been demonstrated to correlate with the amphibole-melt partition coefficient of Ca (Hilyard et al. 2000; Klein et al. 1997; Sisson 1994). These correlations have been used to build empirical models of amphibole-melt REE partition coefficients (Sisson 1994; Tiepolo et al. 2000, 2007). These previous models are useful for predicting the REE and Y partition coefficients when the equilibrium melt composition (Sisson 1994; Tiepolo et al. 2000, 2007) or amphibole-melt major element partition coefficients (Hilyard et al. 2000) are available. These models are difficult to implement, however, for natural amphiboles such as those found in cumulates and xenoliths where melt composition is not available. Furthermore, previous models parameterized partition coefficients for individual elements independently, so each element requires a different set of model coefficients. This makes it difficult to understand the general behavior of REE partitioning in amphibole and to develop accurate models for elements with sparse partitioning data (such as Gd and Tm). In addition, these empirical models require many coefficients to describe the partitioning of all the REEs and Y.

In this study, we present the first parameterized lattice strain models for REE and Y partitioning between amphibole and silicate melt for a range of P, T, melt, and amphibole compositions. These models are developed following a new protocol that has been successfully used to develop parameterized lattice strain models for REE and Y partitioning between major rock-forming minerals (clinopyroxene, orthopyroxene, garnet, olivine, and plagioclase) and basaltic melts (Dygert et al. 2014; Sun et al. 2017; Sun and Liang 2012, 2013a, 2013b; Yao et al. 2012). We develop two parameterized lattice strain models, one of which is described by T and mineral composition, and the other is mostly captured by melt composition. We reconcile the two models through amphibolemelt equilibria, and, as a byproduct, develop a new thermometer for calculating the amphibole liquidus. As geochemical applications of our models, we (1) evaluate the ranges of amphibole-melt REE partition coefficients in mantle amphiboles using observed amphibole compositions in mantle xenoliths and (2) calculate the REE concentration in experimental melts that simulate fractional crystallization of arc magmas to evaluate the effect of amphibole fractional crystallization on the REE concentration in arc magmas.

METHODS

Data compilation

REE and Y partitioning data for amphibole and silicate melts were compiled from published experimental studies. The data were filtered on the basis of attainment of equilibrium (e.g., absence of core to rim variation, sector zoning in major elements, absence of melt inclusions in the analyzed volume, and run duration), misfits or

outliers with reference to the lattice strain model (e.g., Eu anomaly), following the procedure established in the previous studies (Dygert et al. 2014; Sun and Liang 2012, 2013b; Yao et al. 2012). Experimental data that were analyzed using an ion probe and laser ablation-inductively coupled-mass spectrometry (LA-ICP-MS) were inspected for their quality by plotting the partition coefficients of similarly incompatible element pairs (e.g., La-Ce, Eu-Nd, and Lu-Yb, example shown in Supplemental1 Fig. S1). In these plots, most partitioning data follow a well-defined correlation suggesting high-quality and internally consistent analysis while some partitioning data significantly deviate off the trend. The off-trend partitioning data were excluded as they suggest either presence of Eu anomalies, poorly equilibrated experiments, or low-quality analysis. This method could not be used to inspect the quality of highly doped experiments analyzed using an electron microprobe (EMP) as they often contain fewer than three elements that are far from each other in incompatibility. Furthermore, the studies of Adam and Green (1994) and Klein et al. (1997) showed evidence of Henry's law behavior of REEs in their doped experiments by running an undoped experiment at the same P-T-X conditions, while the study of Hilyard et al. (2000) did not show any evidence for this. As shown later in this study, however, the partitioning data of Hilyard et al. (2000) follow our partitioning models in the same manner as other partitioning data, suggesting the Henry's law behavior of REEs in their experiments. Hence, we included the partitioning data from Hilyard et al. (2000) in our data set.

Following the data selection procedure outlined above, we obtained 556 partitioning data from 100 experiments reported in 9 studies (Adam and Green 1994, 2003, 2006; Dalpé and Baker 2000; Hilyard et al. 2000; Klein et al. 1997; LaTourrette et al. 1995; Nandedkar et al. 2016; Tiepolo et al. 2000). Table 1 summarizes the selected partitioning studies that were used to calibrate the model described below. The selected 100 experiments were conducted at 780–1100 °C and 0.2–2.5 GPa. These experiments produced calcic amphiboles and melts with large variations in composition (e.g., Si = 5.74–7.27 apfu in amphibole, Mg# = 36.5–100 in amphibole, Mg# = 1.9–100 in melt, SiO₂ = 34.14–68.7 wt% in melt; see Fig. 1 and Table 1 for details) and partition coefficients (e.g., D_{Lu} = 0.03–0.59, D_{Sm} = 0.27–5.56, D_{Lu} = 0.28–6.77) (Fig. 2). The compositional variations in the experimental amphiboles and melts cover a large portion of those in natural samples from arc and intraplate settings and mantle xenoliths (Figs. 1a–1f).

Parameterization method

To develop a parameterized model for trivalent REE and Y partitioning between amphibole and silicate melt, we conducted a multivariable nonlinear least-squares analysis. Following the procedure of recent studies on mineral-melt REE partitioning (Dygert et al. 2014; Sun and Liang 2012, 2013a, 2013b; Yao et al. 2012; Sun et al. 2017), we conduct the least-squares analysis in two steps: (1) identification of key variables that affect D_0 , r_0 , and E in the lattice strain model through least-squares analysis of individual experiments; and (2) simultaneous inversion of all the filtered experimental data using the primary variables identified in step 1. An important advantage of step 2 is that it allows us to include experiments that reported only one or two trace elements and hence they can be used to calibrate the three-parameter lattice strain model in step 1 [see Supplemental Fig. S2 and S3 for experiments from Hilyard et al. (2000) and Klein et al. (1997)]. We assume that REEs and Y enter the M4 site in amphibole, and use eightfold-coordinated ionic radii from Shannon (1976). We did not distinguish between the M4 and M4' sites (Bottazzi et al. 1999) given the lack of evidence of the two-site occupancy of the REEs in amphibole in our data. We assumed that D_0 in the lattice strain model has the simple form

$$\ln D_0 = a_0 + \frac{a_1}{RT} + f\left(X, \frac{P}{T}\right) \tag{2}$$

where a_0 and a_1 are constants to be determined, and f is a function of mineral and melt composition and P-T. The r_0 is assumed to be a function of mineral composition as it correlates well with the amphibole composition. We explored the composition and r_0 dependence of E observed for other minerals (Sun and Liang 2012, 2013b; Yao et al. 2012), but it shows only small variation for amphibole and does not correlate well with amphibole composition or r_0 . Hence, E was assumed to be a constant.

Through an extensive search of various permutations of the composition vari-

¹Deposit item AM-17-116110, Supplemental Material. Deposit items are free to all readers and found on the MSA web site, via the specific issue's Table of Contents (go to http://www.minsocam.org/msa/ammin/toc/2017/Nov2017_data/Nov2017_data.html).

TABLE 1. Data sources and experimental run conditions

Study	nª	m⁵	P (GPa)	T (°C)	Dur (h)	Amph Mg#	Melt Mg#	Melt SiO ₂ (wt%)	Melt H ₂ O (wt%) ^c
				lon p	robe analys	is			
LaTourrette et al. (1995)	1	10	1.5	1092	17.5	80.3	63.2	44.6	4.27
Tiepolo et al. (2000)	24	222	1.4	950-1075	36	36.5-100	15.1-100	41.5-54.6	2.4-6.15
				LA-IC	P-MS analys	sis			
Dalphe and Baker (2000)	7	88	1.5-2.5	1000-1100	24-100	67.0-93.0	46.4-87.3	34.1-47.1	
Adam and Green (2003)	4	27	0.5-2	1000-1050	24	73.0-78.5	48.1-54.3	39.9-46.0	6.2-13.0
Adam and Green (2006)	2	20	1.0-2.0	1025-1050	48	78.9-80.0	51.2-56.5	39.1-41.4	10.3-14.1
Nandedkar et al. (2016)	8	98	0.7	780-1010	48-100	66.3-77.1	42.2-58.8	51.1-65.9	6.2-9.9
				EN	AP analysis				
Adam and Green (1994)	2	8	2	1050-1100	24	78.3-78.5	60.4-72.0	41.6-43.3	
Klein et al. (1997)	18	27	1	800-900	58-85	55.5-69.0	21.6-45.1	60.5-68.7	
Hilyard et al. (2000)	34	56	0.2-0.5	900–945	70–100	59.3–75.5	1.9-40.2	55.8–67.0	
Total range	100	556	0.2-2.5	780–1100	17.5–100	36.5-100	1.9–100	34.1–68.7	2.4-14.1

^a n represents the number of experiments.

ables, we found that D_0 can be described as a function of melt Si, Ti, and Ca contents or as a function of T and Ti, Mg, Na, and K contents in amphibole. For convenience of description, we refer to the latter as the mineral composition model and the former as the melt composition model. In both models, ferromagnesian (sum of Mg, Fe2+, and Mn²⁺, designated as Fm hereafter) content in the M4 site of the amphibole is the main factor affecting r_0 , while E is a constant. For the melt composition model, the lattice strain parameters D_0 , r_0 , and E take on the following expressions:

$$\ln D_0^{amph} = a_0 + a_1 \ln(X_{Si}^{melt}) + a_2 \ln(X_{Ti}^{melt}) + a_3 \ln(X_{Ca}^{melt})$$
 (3)

$$r_0^{\text{amph}} = a_4 + a_5 X_{\text{Fm}}^{\text{amph-M4}}$$
 (4)

$$E^{\text{amph}} = \mathbf{a}_6. \tag{5}$$

For the mineral composition model, we have

$$\ln D_0^{\rm amph} = b_0 + \frac{b_1}{RT} + b_2 X_{\rm Ti}^{\rm amph} + b_3 X_{\rm Mg}^{\rm amph} + b_4 X_{\rm Na}^{\rm amph} + b_3 X_{\rm K}^{\rm amph}$$

$$r_0^{\rm amph} = b_6 + b_7 X_{\rm Fim}^{\rm amph-M4}$$

$$\tag{7}$$

$$r_0^{\text{amph}} = b_6 + b_7 X_{\text{Fm}}^{\text{amph-M4}} \tag{7}$$

$$r_0^{\text{amph}} = b_6 + b_7 X_{\text{Fm}}^{\text{amph}} \tag{7}$$

$$E^{\text{amph}} = b_8 \tag{8}$$

where a₀, a₁,... a₆ and b₀, b₁,... b₈ in Equations 3-8 are constants determined by stepwise multiple linear regression analyses of the lattice strain parameters (Do, r_0 , and E); $X_{\text{Ti}}^{\text{amph}}$, $X_{\text{Mg}}^{\text{amph}}$, $X_{\text{Na}}^{\text{amph}}$, and $X_{\text{K}}^{\text{amph}}$ are cation numbers (per 23 oxygen) and $X_{\rm Fm}^{\rm amph-M4}$ is the Fe²⁺ + Mn²⁺ + Mg content in the M4 site assuming all iron is present as ferrous iron; and $X_{\text{Si}}^{\text{melt}}$, $X_{\text{Ti}}^{\text{melt}}$, and $X_{\text{Ca}}^{\text{melt}}$ are mole fractions of cations in the melt calculated on an anhydrous basis assuming all iron is present as ferrous iron. The experiments used to parameterize our model were performed at oxygen fugacities between QFM-2 to QFM+3.2 (where QFM is the quartz-fayalite-magnetite buffer), which covers a large range of those found in natural magmatic systems (Ballhaus 1993; Kelley and Cottrell 2009; Parkinson and Arculus 1999), Hence, our assumption of all iron in amphibole and melt being present as ferrous iron is incorrect. Nevertheless, this simplification allows us to develop parameterized lattice strain models for amphibole-melt REE partitioning without making complicated assumptions with regard to the ferric iron content in the amphibole and melt. Also, Na occupies both the M4 and A sites in amphibole, but we use the total Na content for the mineral composition model. We attempted to use Na in the M4 and A sites as separate variables, but the coefficients for the two variables are nearly identical, leading us to use total Na content instead. Finally, we used the anhydrous basis for the melt as another simplification because in some studies, H₂O contents in the melt are calculated according to mass balance, which may introduce large uncertainties. These more complicated but realistic treatment of amphibole and melt compositions should be considered in future studies when knowledge of redox state, site occupancy, and water content becomes available

To further improve the fit to the measured partitioning data and better assess the uncertainties for the fitting coefficients, we performed global least-squares analyses for the melt composition and mineral composition models by substituting Equations 3-5 and 6-8 into Equation 1, respectively. For the melt composition model (Eqs. 1, 3-5), we inverted the 6 coefficients (a₀, a₁,... a₆) simultaneously through a global inversion of the 556 filtered partitioning data. For the mineral composition model (Eqs. 1, 6-8), we inverted the 8 coefficients (b₀, b₁,... b₈) simultaneously through a global inversion of the same data used for the melt composition model. To carry out the global inversions, we used the coefficients from the stepwise multiple linear regression as initial values in the nonlinear least-squares analysis and minimize the

$$\chi_{p}^{2} = \sum_{j=1}^{N} \left(\ln D_{j} - \ln D_{j}^{m} \right)^{2} \tag{9}$$

where D_i is defined by Equation 1 for element j, D_i^m is the measured amphibole-melt partition coefficient for element j, and N (= 556) is the total number of measured partitioning data used in this study. Because it is difficult to assess inter-laboratory uncertainties arising from different experimental procedures and analytical methods in the selected partitioning studies (Table 1), we did not weight the χ^2 using reported uncertainties of measured partition coefficients. The latter are based solely on chemical analysis of REE and Y in individual charges. However, the actual uncertainties in the partition coefficients could be largely due to uncertainties in the experimental conditions (e.g., temperature, oxidation state, water content). Hence, Equation 9 assumes equal uncertainty for all the experimental data included in this study. This is an obvious simplification, but can be judged by the quality of our best fit models for individual samples (see Supplemental Figs. S2 and S3).

Although convenient in nonlinear regression analysis, the absolute values of the χ^2 defined by Equation 9 depend on the number of data used in the inversion. To assess the goodness of fit in a simple way, we calculated the Pearson's Chi-square (χ^2_D) after the inversion using the expression

$$\chi_p^2 = \sum_{j=1}^N \frac{\left(D_j - D_j^m\right)^2}{D_j}.$$
 (10)

A better predictive model should provide partition coefficients closer to measured values and hence has a smaller χ^2_p . The results are shown in Figure 3 and discussed below.

RESULTS

The global fit to the 556 partitioning data from the 100 experiments produces two sets of expressions for the lattice strain parameters for REE and Y partitioning in amphibole. For the melt composition model, we have:

$$\begin{split} &\ln\!D_0^{\rm amph} = -3.08(\pm 0.52) + 0.74(\pm 0.34) ln(X_{\rm in}^{\rm selt}) \\ &- 0.33(\pm 0.05) ln(X_{\rm Ii}^{\rm nelt}) - 0.84(\pm 0.07) ln(X_{\rm Ca}^{\rm nelt}) \quad (11) \\ &r_0^{\rm amph} = 1.045(\pm 0.003) - 0.048(\pm 0.009) X_{\rm fim}^{\rm smph-M4} \end{split} \tag{12}$$

$$E_{\text{amph}} = 241(+10) \tag{12}$$

$$E^{\text{amph}} = 341(\pm 18)$$
 (13)

where r_0 is in angstroms; and E is in GPa; and numbers in parentheses are 25 uncertainties estimated directly from the simultaneous inversion. As D_0 defines the peak value of the parabola in the lattice strain model (Eq. 1), the melt composition model indicates REE partition coefficients in amphibole increase with the increase of Si content in the melt and decrease with the

b m represents the number of partitioning data.

⁶ Melt H2O content shown when reported in the study. It was measured using SIMS by Tiepolo et al. (2000) and LaTourrette et al. (1995), and using micro-Raman spectroscopy by Nandedkar et al. (2016), and calculated using mass balance by Adam and Green (2003, 2006).

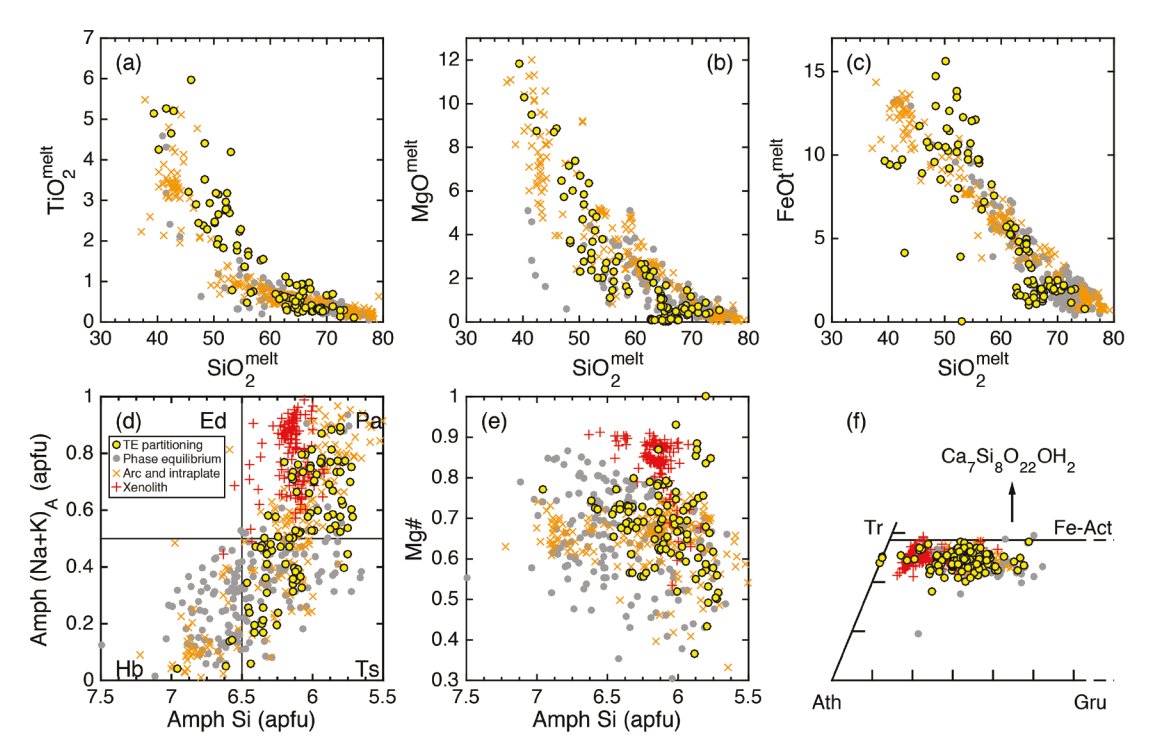


FIGURE 1. Compositions of melt and amphibole in phase-equilibrium experiments (gray dots) and partitioning experiments (yellow dots). Compositions of melt are on anhydrous basis. Also shown are compositions of volcanic rocks and amphiboles in intraplate and arc settings (orange crosses) and xenoliths (red plus signs). The structural formula of amphiboles in panels d and e were calculated using the method of 13 cations excluding Ca, Na, and K described by Leake et al. (1997) for amphibole classification purpose, but for the parameterization procedure, all iron in the amphibole was assumed to be ferrous iron for reasons given in the methods section of the text. The partitioning data are from the compiled experiments in Table 1. Phase equilibrium data from 16 studies (Alonso-Perez et al. 2009; Blatter et al. 2013; Costa et al. 2004; Foden and Green 1992; Gardner et al. 1995; Grove et al. 1997, 2003; Holtz et al. 2004; Kawamoto 1996; Moore and Carmichael 1998; Nandedkar et al. 2014; Nekvasil et al. 2004; Pichavant et al. 2002; Pilet et al. 2010; Prouteau and Scaillet 2003; Sato et al. 2005). Volcanic rocks and amphiboles in intraplate and arc settings from 20 studies (Bernard et al. 1996; Buckley et al. 2006; Costa and Chakraborty 2004; Demény et al. 2004; Gourgaud et al. 1989; Grove et al. 2005; Heliker 1995; Mayer et al. 2013; Mortazavi and Sparks 2004; Neumann et al. 1999; Nye and Turner 1990; Pallister et al. 1996, 2008; Pichavant et al. 2002; Reubi and Nicholls 2004; Ridolfi et al. 2008; Samaniego et al. 2005; Shane et al. 2005; Tappe et al. 2007; Toya et al. 2005) and xenoliths from 10 studies (Chazot et al. 1996, 2005; Grégoire et al. 2000; Ionov and Hofmann 1995; Moine et al. 2001; Vannucci et al. 1995; Vaselli et al. 1995; Witt-Eickschen et al. 2003; Wulff-Pedersen et al. 1996; Zanetti et al. 1996). (Color online.)

increase of Ti and Ca content in the melt. Figures 4a–4c show that the amphibole-melt Sm partition coefficient positively correlates with Si and negatively correlates with Ti and Ca contents in the melt. The Si, Ti, and Ca contents in the experimental melts are comparable to those in the natural melts saturated in amphibole ($SiO_2 = 34.14-68.7$ wt%, $TiO_2 = 0.09-5.39$ wt%, CaO = 1.6-12.89 wt%; data sources in Fig. 1).

For the mineral composition model, we have

$$\begin{split} \ln D_{\scriptscriptstyle 0}^{\rm amph} = & -4.21(\pm 1.20) + \frac{7.27(\pm 0.88) \times 10^4}{\text{R}\,T} + 1.52(\pm 0.24) X_{\rm Ti}^{\rm amph} \\ & -0.35(\pm 0.06) X_{\rm Mg}^{\rm amph} - 1.83\,(\pm 0.34) X_{\rm Na}^{\rm amph} - 2.95(\pm 0.34) X_{\rm K}^{\rm amph} \end{split}$$

$$r_0^{\text{amph}} = 1.043(\pm 0.004) - 0.039(\pm 0.012)X_{\text{Fm}}^{\text{amph-M4}}$$
 (15)

$$E^{\text{amph}} = 337(\pm 23).$$
 (16)

The mineral composition model indicates REE partition coefficients in amphibole increase with the increase of Ti content and decrease with the increase of T and Mg, Na, and K contents in the amphibole. Figure 4d shows a negative correlation between amphibole-melt Sm partition coefficient and T that is consistent

with the expression for D_0 in the mineral composition model (Eq. 14). To highlight the effect of amphibole composition, we subtract the effect of T on the amphibole-melt Sm partition coefficient using the following expression

$$\overline{D_{\text{Sm}}^{\text{amph-melt}}} = D_{\text{Sm}}^{\text{amph-melt}} \exp \left[\frac{4\pi E N_{A}}{RT} \left(\frac{r_{0}}{2} (r_{0} - r_{\text{Sm}})^{2} - \frac{1}{3} (r_{0} - r_{\text{Sm}})^{3} \right) - \frac{7.27 \times 10^{4}}{RT} \right] (17)$$

where $\overline{D_{\rm Sm}^{\rm amph-melt}}$ is the normalized amphibole-melt Sm partition coefficient, r_0 is calculated using Equation 15, and E is that in Equation 16. Figures 4e, 4f, and Supplemental Figure S4 show that, to the first order, normalized amphibole-melt Sm partition coefficient positively correlates with Ti content, and negatively correlates with Mg and K contents in the amphibole, consistent with Equation 14. The negative correlation with Na contents in amphibole is less clear (Fig. S4a), but it is clearer when other compositional effects are subtracted from the normalized amphibole-melt Sm partition coefficient (not shown). The Ti, Mg, Na, and K contents in the experimental amphiboles are comparable to those in natural amphiboles (TiO₂ = 0.73–6.35,

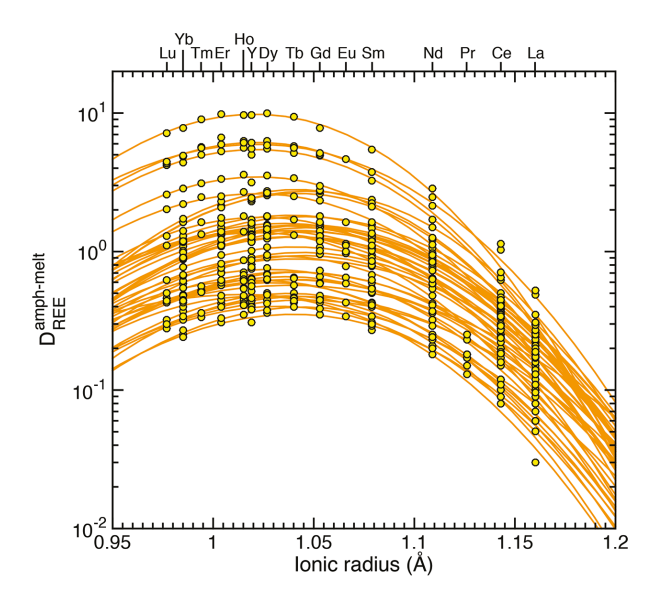


FIGURE 2. Onuma diagram showing the REE and Y partition coefficients between amphibole and silicate melt measured in the partitioning studies listed in Table 1 (yellow dots). The orange lines are the best-fit parabolas to the trivalent REE and Y using the lattice strain model (Blundy and Wood 1994; Brice 1975; Wood and Blundy 1997) for experiments in which there are more than 3 partitioning data. (Color online.)

MgO = 6.35-18.5, Na₂O = 1.20-4.04, and K₂O = 0.03-2.77, all in wt%; data sources in Fig. 1).

In both the mineral and melt composition models, r_0 decreases with increasing Fm content of the M4 site in the amphibole. We interpret this to indicate that the ideal radius of the M4 site decreases with increasing occupancy by elements with relatively small ionic radius such as Mg, Fe²⁺, and Mn²⁺. The range in Fm content of the M4 site in the experimental amphibole is 0–0.58, which exceeds the 0–0.47 observed in the compilation of natural calcic amphiboles (data source in Fig. 1). This range in Fm content of the M4 site in the compilation of natural amphiboles translates to a small range in r_0 of 1.02–1.045 Å (using Eq. 12), which is consistent with the subparallel parabola defined by the REE+Y partitioning data (Fig. 2). Furthermore, the proximity of r_0 to MREE such as Dy (1.027 Å) and Tb (1.04 Å) also explains why fractional crystallization of amphibole can produce depletion in MREEs relative to HREEs and LREEs in the magma (Davidson et al. 2007, 2013). Given the narrow range in Fm content of the M4 site in natural calcic amphiboles, it is reasonable to assume a constant r_0 when using our melt composition model without knowledge of the equilibrium amphibole composition as long as it is expected to be calcic in composition. For natural calcic amphiboles in arcs, non-arcs, and mantle xenoliths, r_0 can be reasonably assumed to be 1.027, 1.04, and 1.039 Å, respectively, based on compilations of natural calcic amphibole composition (data source in Fig. 1).

DISCUSSION

Our mineral composition and melt composition models reproduce the 556 partitioning data from the 100 partitioning experiments (fits to the individual experiments are shown in Supplemental¹ Figs. S2 and S3). The partition coefficients predicted by the melt composition model (Fig. 3a) and the mineral

composition model (Fig. 3b) both follow the 1:1 correlation line when plotted against the measured values and generally fall between the 1:2 and 2:1 correlation lines. Hence to the first approximation, both models equally describe the variability of partition coefficients. In detail, the melt composition model (χ^2_{φ} = 41.3) performs slightly better than the mineral composition model (χ^2_{φ} = 93.7), especially for cases when measured D > 1.

Comparison with the empirical model of Tiepolo et al. (2007)

Our new melt composition model has four variables and seven coefficients for the 15 elements (REE+Y), whereas the melt composition model of Tiepolo et al. (2007), which is a linear fit to one composition variable, has eight coefficients for four elements (La, Dy, Y, and Yb). In terms of reproducing measured partitioning data for these four elements, the Pearson's Chi-square for the original model of Tiepolo et al. (2007) (26.0) is larger than our melt model (11.6 for a fit using La, Dy, Y, and Yb only). To further compare with the model of Tiepolo et al. (2007), we recalibrated their equations for the 15 elements (REE+Y) using our compiled database (Supplemental Table S1 provides the new coefficients). The updated model has a χ^2_ρ value of 54.6, which is still larger than that for our melt model (41.3). Therefore, our melt composition model

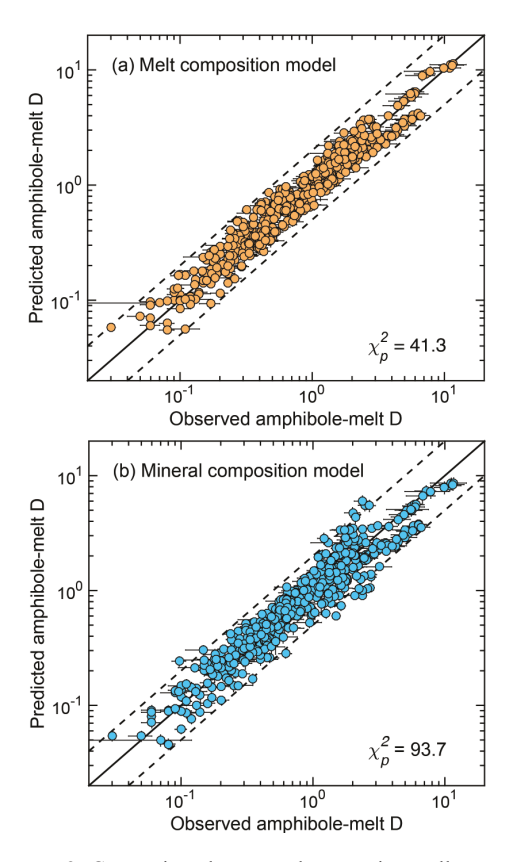


FIGURE 3. Comparison between the experimentally measured partition coefficients to those predicted using (a) the melt composition model (Eqs. 1 and 11–13) and (b) the mineral composition model (Eqs. 1 and 14–16). Observed values are from partitioning studies listed in Table 1. The solid line represents 1:1 ratio, and dashed lines represent 2:1 and 1:2 ratios, respectively. χ_p^2 is the Pearson's Chi-square calculated according to Equation 10. (Color online.)

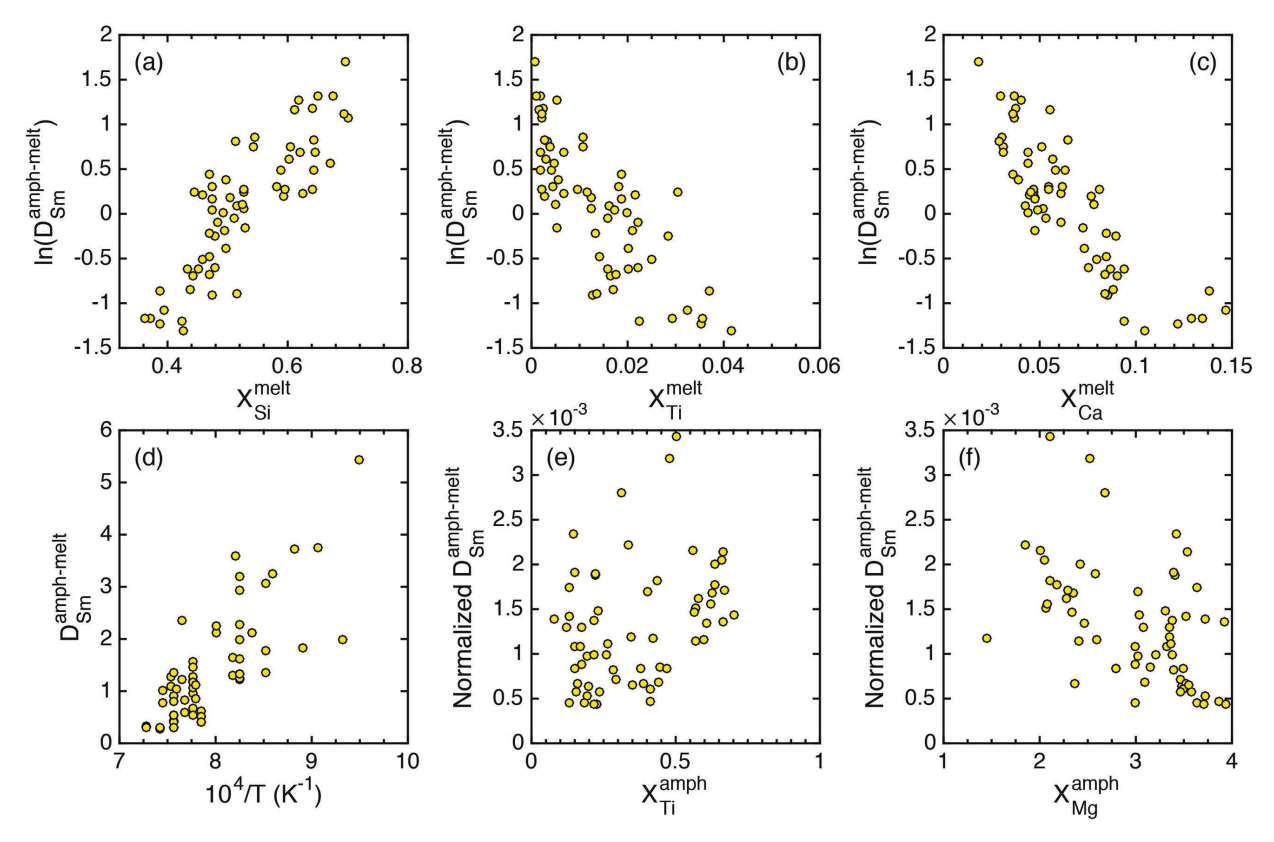


FIGURE 4. Plots of amphibole-melt Sm partition coefficient against mole fractions of (a) Si, (b) Ti, and (c) Ca in the melt and (d) T, (e) Ti, and (f) Mg content in the amphibole. The partition coefficients of Sm in e and f are normalized using Equation 17. The partitioning data are from the compiled experiments in Table 1. (Color online.)

has a better reproducibility and a smaller number of coefficients to describe the REE partitioning between amphibole and silicate melt. This further underscores the advantage and importance of the lattice strain model in quantifying REE partitioning in amphibole. In addition, as shown later in this study, our mineral composition model provides an understanding of the REE substitution mechanism in amphibole, and has the advantage of being applicable to natural samples without the knowledge of the melt composition.

Relation between the mineral composition and melt composition models

The connection between the mineral composition and melt composition models can be understood in terms of amphibole-melt phase equilibria. To within estimated uncertainties, the coefficients in the equations for r_0 and best-fit values for E are identical between the melt composition and mineral composition models (Eqs. 12 vs. 15; Eqs. 13 vs. 16). This implies that D_0 values between the two models are the same, given the two models are equivalent in terms of reproducing measured REE partitioning data (Figs. 3a and 3b). Equating Equations 11 and 14, we have the following expression relating amphibole composition to coexisting melt composition

$$\begin{aligned} &-3.08 + 0.74 \ln(X_{\text{Si}}^{\text{melt}}) - 0.33 \ln(X_{\text{Ti}}^{\text{melt}}) - 0.84 \ln(X_{\text{Ca}}^{\text{melt}}) = \\ &-4.21 + \frac{7.27 \times 10^4}{\text{R}T} + 1.52 X_{\text{Ti}}^{\text{amph}} - 0.35 X_{\text{Mg}}^{\text{amph}} - 1.83 X_{\text{Na}}^{\text{amph}} - 2.95 X_{\text{K}}^{\text{amph}} \end{aligned}$$

Equation 18, in effect, describes the liquidus of amphibole, and hence can be taken as a thermometer for amphibole-melt equilibria, viz.,

$$T = \frac{8.74 \times 10^{3}}{1.13 - 1.52 X_{\text{Ti}}^{\text{amph}} + 0.35 X_{\text{Mg}}^{\text{amph}} + 1.83 X_{\text{Na}}^{\text{amph}} + }{2.95 X_{\text{K}}^{\text{amph}} + 0.74 \ln(X_{\text{Si}}^{\text{melt}}) - 0.33 \ln(X_{\text{Ti}}^{\text{melt}}) - 0.84 \ln(X_{\text{Ca}}^{\text{melt}})}$$
(19)

This thermometer provides an opportunity to independently test our melt composition model (Eqs. 1 and 11–13) and mineral composition model (Eqs. 1 and 14–16) as discussed below.

There are a large number of amphibole-melt phase equilibria studies reported in the literature. Here we use Equation 19 to calculate the temperatures of 185 amphibole-melt phase-equilibrium experiments from 16 studies (Alonso-Perez et al. 2009; Blatter et al. 2013; Costa et al. 2004; Foden and Green 1992; Gardner et al. 1995; Grove et al. 1997, 2003; Holtz et al. 2004; Kawamoto 1996; Moore and Carmichael 1998; Nandedkar et al. 2014; Nekvasil et al. 2004; Pichavant et al. 2002; Pilet et al. 2010; Prouteau and Scaillet 2003; Sato et al. 2005). These experiments were conducted at 730-1130 °C and 0.1-1.5 GPa, generally at lower P-T conditions compared to the REE partitioning experiments. Despite some overlap in composition, these experiments produced calcic amphiboles generally higher in Si and lower in alkalis, and melt with higher SiO₂ content compared to those in the REE partitioning experiments (Fig. 1). The temperatures of these experiments calculated using our thermometer (Eq. 19) and the

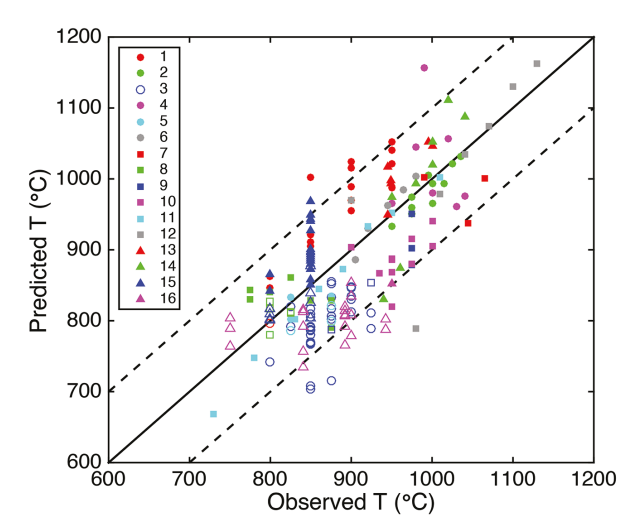


FIGURE 5. Comparison between observed temperatures in phase-equilibrium experiments to those predicted using the thermometer for amphibole-melt equilibria (Eq. 19). Open symbols are experiments containing melts with composition beyond the calibration range of our melt and mineral composition models (SiO₂ higher than 68.7 wt%). Sources of data: (1) Alonso-Perez et al. (2009), (2) Blatter et al. (2013), (3) Costa et al. (2004), (4) Foden and Green (1992), (5) Gardner et al. (1995), (6) Grove et al. (1997), (7) Grove et al. (2003), (8) Holtz et al. (2004), (9) Kawamoto (1996), (10) Moore and Carmichael (1998), (11) Nandedkar et al. (2014), (12) Pilet et al. (2010), (13) Pichavant et al. (2002), (14) Nekvasil et al. (2004), (15) Sato et al. (2005), and (16) Prouteau and Scaillet (2003). (Color online.)

measured temperatures generally follow the 1:1 correlation line to within 100 °C of the measured temperature with a precision of 66 °C (RMSE) (Fig. 5), which is an independent verification of our amphibole-melt thermometer (Eq. 19) and hence our mineral composition and melt composition models. Furthermore, the validity of our thermometer to lower *P-T* conditions and more evolved amphibole and melt composition compared to the REE partitioning experiments suggests the applicability of our models at these conditions.

Our thermometer for amphibole-melt equilibria (Eq. 19) shows similarities to a recent amphibole-melt thermometer of Putirka (2016) that has the expression

$$T(^{\circ}C) = \frac{8037.85}{3.69 + 2.62X_{H,O}^{\text{melt}} + 0.66F_{\text{total}}^{\text{amph}} - 0.416\ln(X_{TiO_{2}}^{\text{melt}}) - 0.37\ln(X_{MgO}^{\text{melt}}) - 1.05\ln(X_{TmO}^{\text{melt}}X_{Al,O_{3}}^{\text{melt}}) - 0.462\ln(D_{Ti})}$$
(20)

where X_1^{melt} are hydrous mole fractions of oxides in the melt, $Fe_{\text{total}}^{\text{amph}}$ is the total Fe cation number in amphibole (per 23 oxygen), and D_{Ti} is the ratio of the Ti cation number in amphibole (per 23 oxygen) divided by the hydrous mole fraction of Ti in the melt. This thermometer and our thermometer both involve the temperature dependence of Ti partitioning between the amphibole and melt. The thermometer of Putirka (2016) has better precision (38 °C) than our thermometer (66 °C) based on the same data set as in Figure 5, but the two thermometers are surprisingly comparable, especially given that our models are calibrated to predict REE partitioning between

amphibole and melt and not temperatures. Therefore, our thermometer captures the essential parameters required in a thermometer for amphibole-melt equilibria.

Substitution mechanism

The mineral composition model may provide insights to the REE substitution mechanism in amphibole. According to the mineral composition model, D_0 positively correlates with Ti and negatively with Mg. Hence REE substitution is related to the Ti–Aliv substitution in the M1,2,3 and tetrahedral sites. Furthermore, the model may suggest that REE substitution for Na in the M4 site is charge compensated by vacancies in the A site, given the negative correlation between Na and K contests in amphibole and D_0 . Taken together, the mineral composition model suggests the following substitution mechanism of REE in amphibole

$$Si_{T}^{4+}Mg_{M_{1}-3}^{2+}Na_{M4}^{1+}3(Na_{A}^{1+},K_{A}^{1+}) \leftrightarrow Al_{T}^{3+}Ti_{M_{1}-3}^{4+}REE_{M4}^{3+}3\square_{A}.$$
 (21)

According to this substitution mechanism, REE partition coefficients should positively correlate with Al^T similar to that observed in clinopyroxene (e.g., Lo Casio et al. 2008; Gaetani and Grove 1995; Hill et al. 2000; Lundstrom et al. 1998; Wood and Blundy 1997). There is a weak positive correlation between Al^T and normalized amphibole-melt Sm partition coefficient (Supplemental¹ Fig. S4c), and its scatter may be due to the effect of variation in other mineral compositions (e.g., Ti, Mg, Na, and K) similar to that observed for Na content in the mineral composition model (Supplemental¹ Fig. S4a). A mineral composition model with Al^T, Mg, Na, and K contents in the amphibole as compositional variables for D_0 has a Pearson's Chi-square of 117, which is higher than our preferred mineral composition model (93.7). Although Al^T plays an important role in REE substitution in amphibole, in practice our mineral composition model performs slightly better when we use Ti rather than Al^T as a compositional variable.

APPLICATIONS

Melting of amphiboles in the mantle

Amphibole is often observed in mantle xenoliths brought to the surface by basalt volcanism, suggesting the presence of hydrated and metasomatized mantle lithosphere (e.g., Boettcher and O'Neil 1980; Chazot et al. 1996; Ionov and Hofmann 1995). Partial melting of such mantle can give rise to melts with a range of compositions (e.g., alkali basalts to nephelinites) (e.g., Médard et al. 2006; Pilet et al. 2008; Sorbadere et al. 2013). In general, major element compositions in mantle amphiboles vary considerably (Figs. 1d-1f). According to the data compiled from 10 studies shown in Figure 1, TiO₂ in amphiboles found in mantle xenoliths varies from 0.15 to 5.94 wt%, MgO from 9.82 to 19.43 wt%, Na₂O from 2.31 to 4.3 wt%, and K from 0 to 2.05 wt%. Based on our mineral model, we expect considerable variability in amphibolemelt REE partition coefficients. For purpose of demonstration, we calculated the amphibole-melt REE partition coefficients in amphiboles found in mantle xenoliths from the 10 studies listed in Table 1 using the mineral composition model for a temperature of 1000 °C. As shown in Figure 6, amphibole-melt REE partition coefficients in amphiboles found in xenoliths vary by nearly an order of magnitude, purely due to their compositional variation. Furthermore, the REE partition coefficients decrease more than

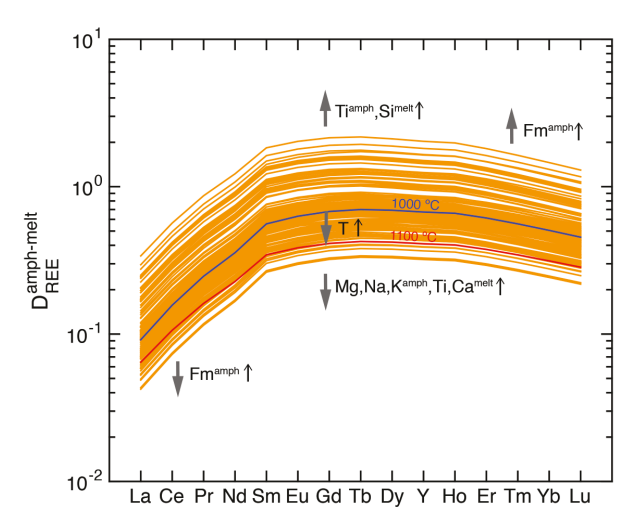


FIGURE 6. Amphibole-melt REE partition coefficients calculated using the mineral composition model (Eqs. 1 and 14–16) and compositions of for amphiboles found in mantle xenoliths. All except the red curve labeled $1100\,^{\circ}$ C were calculated assuming a temperature of $1000\,^{\circ}$ C. The general effects of T and amphibole and melt composition on the amphibole-melt REE partition coefficients are also shown. Data source is the same as those in Figure 1. (Color online.)

20% when the temperature is increased to 1100 °C (cf. heavy blue and red lines in Fig. 6). Despite the large range in REE partition coefficient, its pattern does not noticeably change due to the small range in Fm content in the M4 site of the amphiboles. This simple example demonstrates the importance of composition- and temperature-dependent amphibole-melt REE partition coefficients to geochemical modeling of melting of an amphibole-bearing lithology in the mantle. For convenience, we list in Table 2 the average, maximum, and minimum REE partition coefficients between amphiboles in mantle xenoliths and melt calculated using the mineral composition model at four selected temperatures.

Fractional crystallization of arc magmas

Fractional crystallization of amphibole and clinopyroxene in arc magmas has been postulated to decrease Dy/Yb and Dy/Dy* $[Dy_N/(La_N^{4/13}Yb_N^{9/13})]$ ratios (i.e., depletion in MREEs relative to HREEs and LREEs) with increasing SiO₂ content, as observed in rock samples from single arc volcanoes (Davidson et al. 2007, 2013). However, given the large range in published mineral-melt partition coefficients, the relative importance of amphibole and clinopyroxene in producing low-Dy/Yb and Dy/Dy* ratios in arc magmas is not clear. To better understand this, we use REE partitioning models and mass-balance calculations to estimate and compare the effects of amphibole and clinopyroxene fractional crystallization on the REE patterns of experimental melts compositionally similar to arc magmas (Nandedkar 2014; Nandedkar et al. 2014). The experiments of Nandedkar et al. (2014) and Nandedkar (2014) simulate fractional crystallization of the same initial starting material at pressures of 0.7 and 0.4 GPa, respectively. [Hereafter we refer to the experiments of Nandedkar et al. (2014) as the 0.7 GPa experiments and those of Nandedkar (2014) as the 0.4 GPa experiments.] The initial starting material in these experiments is an olivine-tholeiite with an Mg# of 73 and H₂O content of 3 wt%, and both experiments were run at an oxygen fugacity of Ni-NiO. The experimental temperatures of the 0.7 and 0.4 GPa experiments range from 1170 to 700 and 1110 to 920 °C, respectively. The final amounts of fractional crystallization are 85 wt% for the 0.7 GPa experiments and 76 wt% for the 0.4 GPa experiments. Both experiments crystallized clinopyroxene, olivine, plagioclase, and magnetite, but the 0.7 GPa experiment also crystallized amphibole with less plagioclase. This may be due to the greater stability of amphibole and the lesser stability of plagioclase at high pressure (Allen and Boettcher 1983; Nandedkar 2014; Spulber and Rutherford 1983). Hence, the comparison between the model REE patterns and abundances in the melts of these experiments using REE partitioning models and mass-balance calculations provide an insight into the effect of fractional crystallization on the REE pattern of arc magmas under different P-T conditions and crystallizing phases. Particularly interesting is the effect of amphibole fractional crystallization, which may play a key role in the depletion of MREEs relative to HREEs in arc magmas (Davidson et al. 2007, 2013).

We used the temperature, mineral, and melt composition in the 0.7 and 0.4 GPa experiments to calculate the amphibole-melt and clinopyroxene-melt REE partition coefficients using the melt composition model of this study and the model of Sun and Liang (2012). The amphibole-melt REE partition coefficients in the 0.7 GPa experiments were measured by Nandedkar et al. (2016), and they are part of the partitioning data used for our model calibration. However, we chose to use our models to calculate the amphibole-melt REE partition coefficients to understand what parameters cause changes in the partition coefficients between different experimental runs. The calculated amphibole-melt MREE and HREE partition coefficients in the 0.7 GPa experiments increase by approximately an order of magnitude from the highest to lowest temperature experiment due to the increase in Si, and decrease in Ti and Ca content in the melt (Fig. 7a). In contrast to the MREE and HREE, the LREE partition coefficients do not vary significantly because elements with larger ionic radius relative to r_0 become more incompatible with decreasing temperature (Eq. 1), and this counteracts the increase in D_0 . A calculation using the mineral composition model from this study also predicts an increase in MREE and HREE partition coefficients with progressive fractional crystallization largely due to the decrease in temperature, but also due to the decrease in Na and K content in the amphibole. However, the increase of partition coefficients is a factor of 2 smaller than that predicted by the melt composition model at 730 °C. The disagreement between the models is likely due to the low-crystallization temperature (730 °C), which is below the model calibration range (780-1100 °C). (The amphibole formed at 730 °C is cummingtonite unlike the magnesio-hornblende formed at slightly higher temperature of 780 °C, which may give rise to a different REE substitution mechanism than those described than those described above. We suspect kinetics may also play a role in controlling major element compositions in amphiboles at lower temperatures). Hence caution should be exercised when extrapolating our models to T-X conditions outside the calibration range (Table 1). At temperatures higher than 730 °C, the differences between the amphibole-melt REE partition coefficients predicted by the two models are all within 34%, and the results discussed in the rest of this section are not model dependent. The

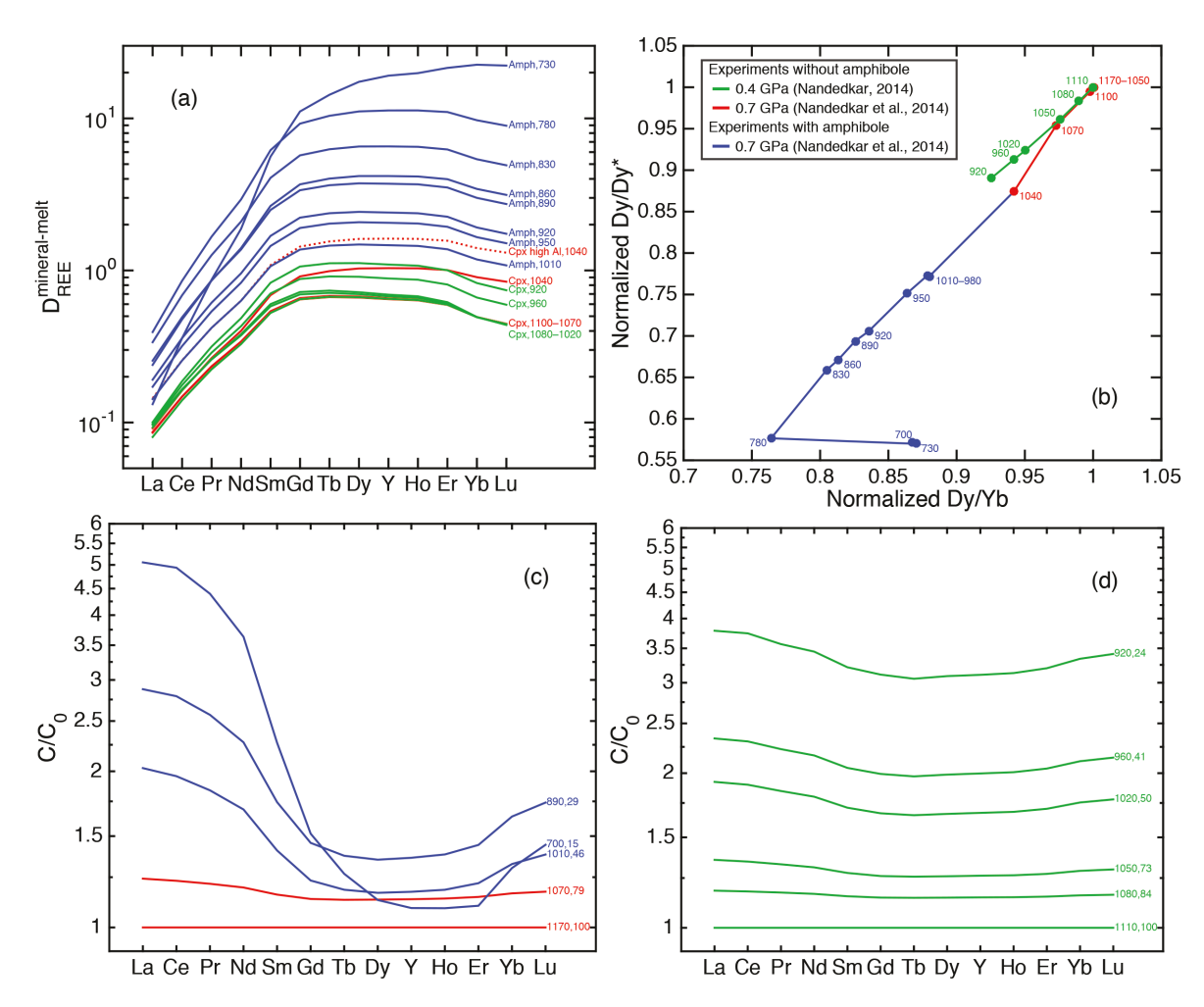


FIGURE 7. (a) Predicted amphibole-melt (blue lines) and clinopyroxene-melt (red and green lines) REE partition coefficients for mineral and melt compositions reported in the studies of Nandedkar et al. (2014) (0.7 GPa experiments, blue and red lines) and Nandedkar (2014) (0.4 GPa experiments, green lines), calculated using the melt composition model for amphibole-melt and the model of Sun and Liang (2012) for the clinopyroxene-melt. The dotted red line is the clinopyroxene-melt REE partition coefficient for a high-Al clinopyroxene found in the 0.7 GPa experiment at 1040 °C. Numbers on the right of each line are the experimental temperatures in degrees Celsius. (b) Dy/Dy* vs. Dy/Yb ratios (Davidson et al. 2013) and (c-d) REE concentrations in the 0.7 and 0.4 GPa melts normalized to those in the initial melt calculated using the predicted mineral-melt partition coefficients (melt composition model, Eqs. 1 and 11–13 for amphibole) and consideration of mass balance. Subsets of the experiments are shown for clarity. In b, red circles are 0.7 GPa melts saturated in clinopyroxene, blue circles are those saturated in amphibole, and the green circles are the 0.4 GPa melts with the experimental temperatures in degrees Celsius. For c and d the numbers on the right of each line are the experimental temperatures in degrees Celsius, and the cumulative percentage of the melt that has not been crystallized. (Color online.)

range in clinopyroxene-melt REE partition coefficients in the 0.7 and 0.4 GPa experiments are similar to each other except for the high-Al clinopyroxene found in the 0.7 GPa experiment at 1040 °C. The olivine-melt, opx-melt, and plagioclase-melt REE partition coefficients are calculated using the models of Sun and Liang (2013b), Yao et al. (2012), and Sun et al. (2017), respectively. The spinel-melt REE partition coefficients are from Kelemen et al. (2003). The other phases such as apatite and magnetite were not considered for simplicity.

The partition coefficients and the phase proportions in the 0.7 and 0.4 GPa experiments (Nandedkar 2014; Nandedkar et al. 2014) were used to model the REE abundances in the melts during fractional crystallization. The model results are shown in in Figures 7b, 7c, and 7d. The Dy/Dy* and Dy/Yb ratios of the 0.7 GPa melt

decrease significantly more than those of the 0.4 GPa melt during fractional crystallization (Fig. 7b). Furthermore, the 0.7 GPa melts are more depleted in MREEs and HREEs compared to the 0.4 GPa melts for a given degree of fractional crystallization (Figs. 7c and 7d). These differences are due to fractional crystallization of amphibole in the 0.7 GPa melts. As shown in the results section, amphibole fractional crystallization decreases the Dy/Dy* and Dy/Yb ratios in the melt due to the affinity of amphibole for MREEs over HREEs and LREEs (i.e., similarity between r_0 of the amphibole and ionic radius of MREEs) (Figs. 2 and 7a). In addition, amphibole fractional crystallization moderates the MREE and HREE concentration in the melt because they behave compatibly in amphiboles, especially in those crystallizing from more evolved melts (i.e., high Si) at lower temperatures (Fig. 7a). In contrast,

TABLE 2. List of recommended amphibole-melt REE and Y partition coefficients for amphiboles found in xenoliths

Temperature (°C)	1100			1000			900			800		
	Min	Average	Max									
La	0.03	0.078	0.235	0.042	0.112	0.339	0.064	0.17	0.52	0.104	0.28	0.863
Ce	0.049	0.127	0.379	0.073	0.189	0.566	0.115	0.302	0.907	0.197	0.523	1.586
Pr	0.075	0.192	0.563	0.115	0.294	0.868	0.189	0.486	1.442	0.339	0.881	2.631
Nd	0.106	0.266	0.773	0.167	0.42	1.223	0.282	0.715	2.091	0.527	1.343	3.951
Sm	0.162	0.397	1.127	0.263	0.645	1.836	0.463	1.138	3.25	0.906	2.235	6.4
Eu	0.182	0.439	1.237	0.297	0.72	2.03	0.529	1.283	3.624	1.047	2.547	7.209
Gd	0.195	0.467	1.303	0.321	0.769	2.147	0.575	1.378	3.851	1.147	2.753	7.704
Tb	0.201	0.477	1.318	0.332	0.786	2.174	0.596	1.411	3.905	1.194	2.827	7.821
Dy	0.2	0.468	1.283	0.329	0.77	2.111	0.59	1.381	3.782	1.181	2.761	7.552
Υ	0.195	0.454	1.238	0.321	0.746	2.031	0.574	1.333	3.626	1.145	2.656	7.214
Но	0.192	0.445	1.209	0.315	0.729	1.981	0.562	1.301	3.529	1.12	2.587	7.002
Er	0.179	0.413	1.114	0.293	0.673	1.813	0.52	1.193	3.206	1.029	2.352	6.304
Tm	0.165	0.377	1.011	0.268	0.61	1.632	0.472	1.073	2.86	0.925	2.095	5.566
Yb	0.15	0.341	0.909	0.242	0.548	1.456	0.423	0.955	2.528	0.821	1.844	4.862
Lu	0.136	0.308	0.816	0.218	0.491	1.296	0.378	0.847	2.228	0.726	1.617	4.235

Notes: Calculated at different temperatures using the mineral composition model of this study and compositions of for amphiboles found in mantle xenoliths (data source in Fig. 1). The compositions of amphiboles are kept constant for the calculation at different temperatures.

the Dy/Dy* and Dy/Yb ratios do not decrease as much and the MREE and HREE concentrations are significantly higher in the 0.4 GPa melts than the 0.7 GPa melts because they do not crystallize amphibole (Fig. 7b). To some extent, the Dy/Dy* and Dy/Yb ratios in the 0.4 GPa melts decrease due to clinopyroxene fractional crystallization (Fig. 7b), but by much less than the 0.7 GPa melts, because REEs are incompatible in the crystallizing clinopyroxenes especially at high temperatures (Fig. 7a). In contrast, amphibole can significantly fractionate the REE pattern of the 0.7 GPa melts due to the lower crystallization temperatures in the 0.7 GPa melts compared to the 0.4 GPa melts for a given degree of fractional crystallization, perhaps due to the larger temperature difference between the solidus and liquidus at higher pressure.

Applying the present REE partitioning model (melt composition model) to the 0.7 GPa experiments by Nandedkar et al. (2014) suggests that the amphibole-melt REE partition coefficient can vary by an order of magnitude during fractional crystallization of an arc magma due to changes in T, and the melt and amphibole compositions. This range of values demonstrates the importance of composition- and temperature-dependent REE partition coefficients in geochemical modeling of amphibole-melt fractionation. For convenience, we list the amphibole-melt REE partition coefficients for amphiboles in the 0.7 GPa experiments calculated using the melt composition model (Table 3). Our modeling results suggest that fractional crystallization of amphibole plays a key role in decreasing the Dy/Yb and Dy/Dy* ratios and also in moderating the MREE and HREE concentrations in arc magmas. Fractional crystallization of clinopyroxene can also decrease the Dy/Yb and Dy/Dy* ratios in the arc magmas, although much less efficiently. The pressure of fractional crystallization affects the crystallization temperature of the melt and stability of amphibole (Allen and Boettcher 1983; Nandedkar 2014; Spulber and Rutherford 1983), so it is also a key factor that controls the behavior of REE in solidifying magmas.

Our model results suggest that arc magmas that crystallize amphibole should have a fairly restricted range in MREE and HREE concentrations and low-Dy/Yb and Dy/Dy* ratios compared to those that do not crystallize amphibole (Fig. 7). As an example of geological application, we compare two sets of samples from single arc volcanoes, one in which these characteristics are present and another in which they are not. Samples from Mt. Pelée in the Lesser Antilles Arc (Davidson and Wilson 2011) (Fig. 8a) show

the effects of fractional crystallization of amphibole, while those from Anatahan Island in the Mariana Arc (Wade et al. 2005) (Fig. 8b) do not. The samples from Mt. Pelée have a fairly restricted range in MREE and HREE concentrations compared to those from Anatahan Island despite the similar range in bulk SiO₂ content (51-63 wt% for Mt. Pelée and 49-66 wt% for Anatahan Island) and other major element contents (Supplemental Fig. S5) suggesting similar range in degrees of fractional crystallization between the two sets of samples. To the first order, REE and Y concentrations in the samples from Mt. Pelée and Anatahan Island can be fairly well reproduced using the model REE and Y concentrations in subsets of the 0.7 GPa experiments (Nandedkar et al. 2014) and 0.4 GPa experiments (Nandedkar 2014) that have the most similar major element concentrations to those in the samples (Fig. S5) and assuming the REE and Y concentrations in the initial melts are those in the samples with lowest SiO₂ contents. The model REE and Y concentrations also reproduce the greater decrease in Dy/Dy* and Dy/Yb ratios in the samples from Mt. Pelée compared to those from Anatahan Island (Figs. 8c and 8d). Although scatter in the data (Figs. 8c and 8d) and variation in the isotopic composition may suggest some amount of source variation and/or crustal contamination (Davidson and Wilson 2011), the model results suggest amphibole fractional crystallization associated with Mt. Pelée samples but not the Anatahan Island samples. The *P-T-X* conditions of the equilibrium crystallization experiments designed for studying the Mt. Pelée samples (Martel et al. 1998, 1999; Pichavant et al. 2002) are a more accurate representation of those in the Mt. Pelée magma chamber, but we chose to use the 0.7 GPa experiments (Nandedkar et al. 2014) as they are fractional crystallization experiments that allows continuous modeling of the effects of changing temperature and melt/mineral composition on the REE concentration in a crystallizing melt. A combination of fractional crystallization experiments ran at relevant P-T-X conditions and the REE partitioning models for amphibole and other mineral phases (Dygert et al. 2014; Sun et al. 2017; Sun and Liang 2012, 2013b; Yao et al. 2012) may be useful for unraveling the P-T conditions and variations in major and REE abundance of sets of samples from single arc volcanoes.

CONCLUDING REMARKS

The partitioning of rare earth elements between amphibole and silicate melt depends on temperature, and amphibole and

TABLE 3. List of recommended amphibole-melt REE and Y partition coefficients f	or arc magma environment
---	--------------------------

Temperature (°C)	1010	950	920	890	860	830	780	730 ^a
La	0.14	0.17	0.19	0.25	0.24	0.34	0.39	0.13
Ce	0.26	0.32	0.36	0.49	0.48	0.69	0.85	0.36
Pr	0.42	0.54	0.61	0.86	0.86	1.26	1.67	0.87
Nd	0.63	0.83	0.96	1.37	1.4	2.1	2.93	1.88
Sm	1.07	1.45	1.69	2.5	2.66	4.06	6.18	5.6
Eu	1.24	1.7	1.98	2.97	3.21	4.95	7.77	8.13
Gd	1.37	1.9	2.22	3.37	3.68	5.71	9.23	11.1
Tb	1.46	2.03	2.38	3.63	4.02	6.26	10.4	14.3
Dy	1.48	2.08	2.43	3.74	4.18	6.53	11.11	17.39
Ϋ́	1.47	2.06	2.4	3.72	4.18	6.54	11.27	19.09
Но	1.45	2.04	2.38	3.68	4.15	6.5	11.28	19.84
Er	1.38	1.94	2.26	3.51	3.98	6.24	11.01	21.48
Tm	1.28	1.8	2.09	3.27	3.73	5.85	10.44	22.34
Yb	1.18	1.65	1.92	3	3.44	5.38	9.72	22.53
Lu	1.08	1.51	1.74	2.73	3.14	4.91	8.95	22.24

Notes: Calculated using the melt composition model and the composition of amphiboles in the 0.7 GPa experiments of Nandedkar et al. (2014). The set of partition coefficient at 730 °C should be used with caution since the temperature is below the calibration range of our model.

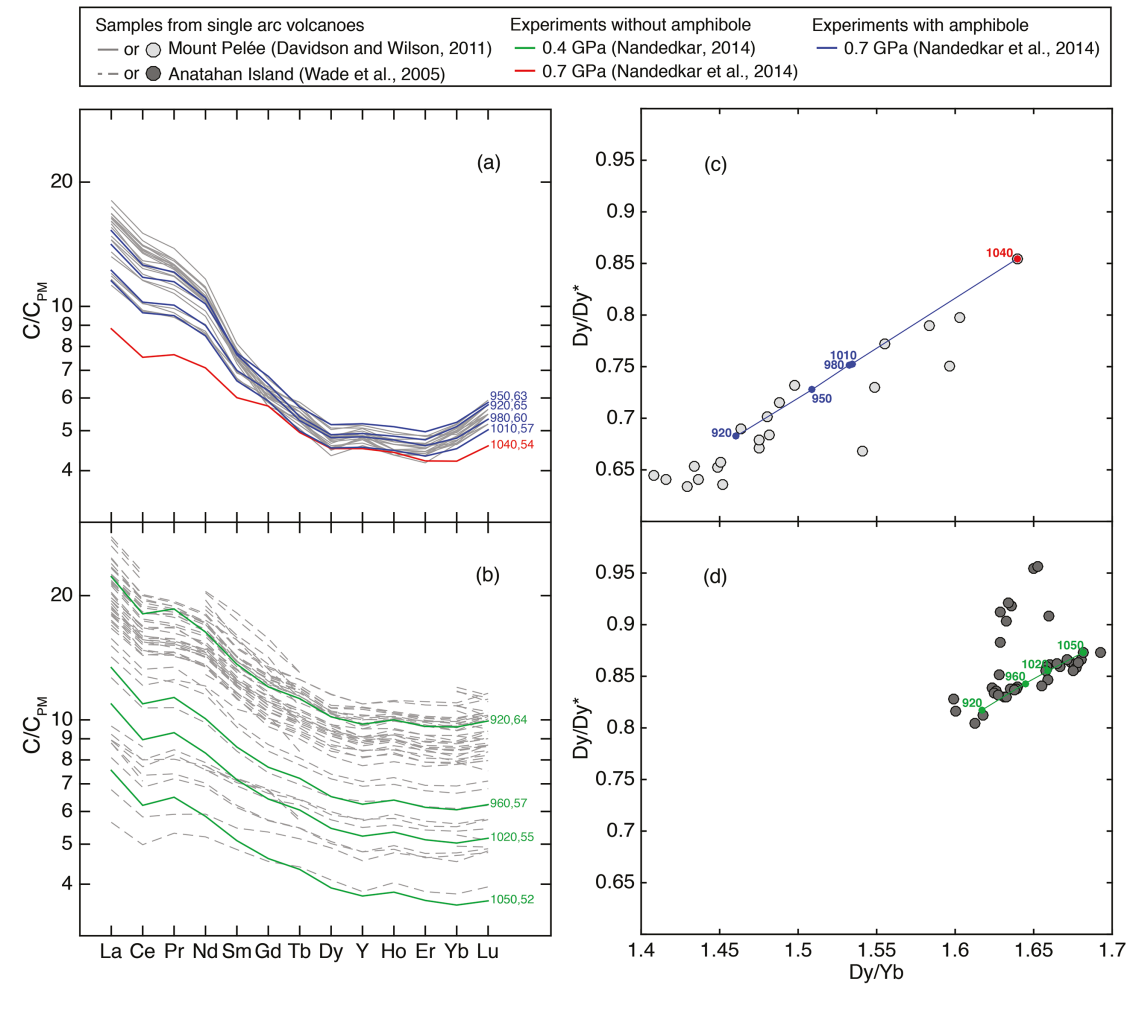


FIGURE 8. Primitive mantle normalized REE concentrations and Dy/Dy* vs. Dy/Yb ratios in samples from (a and c) Mt. Pelée in the Lesser Antilles Arc (Davidson and Wilson 2011) and (b and d) Anatahan Island in the Mariana Arc (Wade et al. 2005). Also plotted are those in the (a and c) 0.7 GPa melts (Nandedkar et al. 2014) and the (b and d) 0.4 GPa melts (Nandedkar 2014) calculated using the predicted mineral-melt partition coefficients (melt composition model, Eqs. 1 and 11–13 for amphibole), consideration of mass balance, and assuming the REE concentration in the initial melts of those in the samples with lowest SiO₂ contents. Subsets of experiments with similar major element concentrations to those in the samples (Supplemental¹ Fig. S5) were used for the calculation. For a and b, the numbers associated with each line correspond to experimental temperatures in degrees Celsius, and the SiO₂ content in the experimental melts (on an anhydrous basis). For c, red circles are 0.7 GPa melts saturated in clinopyroxene, blue circles are those saturated in amphibole, and in d the green circles are the 0.4 GPa melts with the experimental temperatures in degrees Celsius. Primitive mantle values are from McDonough and Sun (1995). (Color online.)

melt compositions. We developed two parameterized lattice strain models for REE and Y partitioning between amphibole and silicate melt over a large range of P-T-X using published partitioning data between amphibole and silicate melt and nonlinear least-squares regression method. The melt composition model suggests that REE and Y partition coefficients in amphibole positively correlate with Si content, and negatively correlate with Ti and Ca contents in the melt. The mineral composition model suggests that REE and Y partition coefficients in amphibole negatively correlate with T and Mg, Na, and K contents and positively correlate with Ti content in amphibole. In both the mineral and melt composition models, r_0 negatively correlates with the Fm content in the M4 site of amphibole and E is a constant. The very similar coefficients of the equations for r_0 and best-fit values for E in the two models suggest that the D_0 in the two models are equivalent. Hence there are considerable trade-offs between major element compositions of coexisting amphibole and melt in the parameterized lattice strain models for REE partitioning in amphibole. The connection is the liquidus surface of amphibole. To further demonstrate this point, we developed a hybrid model for amphibole-melt REE partitioning using a combination of amphibole and melt compositions and the results are summarized in Appendix¹ A. The hybrid model, which performs slightly better than the melt composition model and the mineral composition model, can be used to predict REE partition coefficients if major element compositions of both amphibole and melt are available.

Application of our mineral composition model to amphiboles found in mantle xenoliths suggests an order of magnitude variation in the amphibole-melt REE partition coefficients purely due to compositional variation. Application of our melt composition model to fractional crystallization experiments of arc magma (Nandedkar 2014; Nandedkar et al. 2014) suggests that REE partition coefficients between amphibole and melt can increase by an order of magnitude due to a combined effect of decreasing T and varying amphibole (e.g., decrease in Na and K) and melt compositions (e.g., increase in Si) within this environment. In contrast, r_0 of the crystallizing amphiboles does not change significantly and remains similar to the ionic radius of MREE such as Dy and Tb. Therefore, fractional crystallization of amphibole can play a key role in buffering the REE concentrations in arc magmas, and also in depleting its MREEs relative to HREEs and LREEs.

IMPLICATIONS

Our new mineral composition model is a useful tool to estimate the REE and Y concentration in silicate melt that is in equilibrium with amphibole. Previous models of amphibole-melt REE partition coefficients (Hilyard et al. 2000; Sisson 1994; Tiepolo et al. 2007, 2000) require the major element composition of the melt that is in equilibrium with amphibole, which is not always available for natural samples such as cumulates. Studies on amphibole-bearing rocks (e.g., Davidson and Wilson 2011; Peters et al. 2017) had to choose a set of amphibole-melt trace element partition coefficients from the literature to estimate the trace element concentration in the equilibrium melt. The new mineral composition model developed in the present study is useful in such instances as it only requires the amphibole composition (i.e., Ti, Mg, Na, and K contents) and temperature. Here temperature can be estimated using the amphibole composition-

dependent thermometer of Putirka (2016). The application of the mineral composition model on amphibole-bearing cumulates would allow estimation of the REE concentration in the melt that is in equilibrium with the amphibole-bearing cumulate, which is a useful information for understanding the origin of the cumulates and the effect of its crystallization on evolution of the trace element concentration in the melt. It can also be used to model processes such as formation of amphibole by reaction-replacement of clinopyroxene observed in cumulates (Smith 2014), which may be an important process for explaining the rarity of amphibole phenocrysts in arc lavas, i.e., amphibole being a "cryptic" fractionating phase (Davidson et al. 2007).

Applications of the new amphibole-melt REE partitioning models demonstrate the significantly stronger effect of amphibole fractional crystallization, relative to clinopyroxene fractional crystallization, on buffering the MREE and HREE concentrations and decreasing Dy/Yb and Dy/Dy* ratios in arc magmas (Davidson et al. 2007, 2013). The magnitude of decrease in Dy/Yb and Dy/Dy* ratios found in the samples from Mt. Pelée consistent with amphibole fractional crystallization, is also observed in many other sets of samples from single arc volcanoes (Fig. 7 in Davidson et al. 2013). This suggests that fractional crystallization of amphibole in arc magmas is a common process, which is consistent with its common observation in arc cumulates (e.g., Beard 1986; DeBari and Coleman 1989; Jagoutz et al. 2009; Lapierre et al. 1992; Larocque and Canil 2010). Our study implies that REEs are especially enriched in amphibole-rich cumulates that crystallize from the most differentiated arc magmas, because amphibole-melt REE partition coefficient increases with increasing differentiation of arc magmas.

ACKNOWLEDGMENTS

We thank Othmar Müntener for useful discussion and for sharing amphibole-melt partitioning data. This paper is benefited from thoughtful review comments by Stefan Peters and Calvin Barnes. This work was supported by NSF grants OCE-1355932 and EAR-0810191 (to A.E.S.) and EAR-1624516 (to Y.L.), and a Dissertation Fellowship at Brown University (to K.S.).

REFERENCES CITED

- Adam, J., and Green, T.H. (1994) The effects of pressure and temperature on the partitioning of Ti, Sr and REE between amphibole, clinopyroxene and basanitic melts. Chemical Geology, 117(1), 219–233.
- ——— (2003) The influence of pressure, mineral composition and water on trace element partitioning between clinopyroxene, amphibole and basanitic melts. European Journal of Mineralogy, 15(5), 831–841.
- —— (2006) Trace element partitioning between mica- and amphibole-bearing garnet lherzolite and hydrous basanitic melt: 1. Experimental results and the investigation of controls on partitioning behaviour. Contributions to Mineralogy and Petrology, 152(1), 1–17.
- Allen, J.C., and Boettcher, A.L. (1983) The stability of amphibole in andesite and basalt at high pressures. American Mineralogist, 68, 307–314.
- Alonso-Perez, R., Müntener, O., and Ulmer, P. (2009) Igneous garnet and amphibole fractionation in the roots of island arcs: experimental constraints on andesitic liquids. Contributions to Mineralogy and Petrology, 157(4), 541–558.
- Ballhaus, C. (1993) Redox states of lithospheric and asthenospheric upper mantle. Contributions to Mineralogy and Petrology, 114(3), 331–348.
- Beard, J.S. (1986) Characteristic mineralogy of arc-related cumulate gabbros: implications for the tectonic setting of gabbroic plutons and for andesite genesis. Geology, 14(10), 848–851.
- Bernard, A., Knittel, U., Weber, B., Weis, D., Albrecht, A., Hattori, K., Klein, J., and Oles, D. (1996) Petrology and geochemistry of the 1991 eruption products of Mount Pinatubo. In R.S. Punongbayan and C.G. Newhall, Eds., Fire and Mud: Eruptions and lahars of Mount Pinatubo, Philippines, 767–797. University of Washington Press, Seattle.
- Blatter, D.L., Sisson, T.W., and Hankins, W.B. (2013) Crystallization of oxidized, moderately hydrous arc basalt at mid- to lower-crustal pressures: Implications for andesite genesis. Contributions to Mineralogy and Petrology, 166(3), 861–886.

- Blundy, J., and Wood, B. (1994) Prediction of crystal-melt partition coefficients from elastic moduli. Nature, 372, 452–454.
- Boettcher, A.L., and O'Neil, J.R. (1980) Stable isotope, chemical, and petrographic studies of high-pressure amphiboles and micas: evidence for metasomatism in the mantle source regions of alkali basalts and kimberlites. American Journal of Science. 280-A. 594-621.
- Bottazzi, P., Tiepolo, M., Vannucci, R., Zanetti, A., Brumm, R., Foley, S.F., and Oberti, R. (1999) Distinct site preferences for heavy and light REE in amphibole and the prediction of Amph/LD_{REE}. Contributions to Mineralogy and Petrology, 137(1-2), 36-45.
- Brenan, J.M., Shaw, H.F., Ryerson, F.J., and Phinney, D.L. (1995) Experimental determination of trace-element partitioning between pargasite and a synthetic hydrous andesitic melt. Earth and Planetary Science Letters, 135(1), 1–11.
- Brice, J.C. (1975) Some thermodynamic aspects of the growth of strained crystals. Journal of Crystal Growth, 28(2), 249–253.
- Brophy, J.G. (2008) A study of rare earth element (REE)–SiO₂ variations in felsic liquids generated by basalt fractionation and amphibolite melting: a potential test for discriminating between the two different processes. Contributions to Mineralogy and Petrology, 156(3), 337–357.
- Buckley, V.J.E., Sparks, R.S.J., and Wood, B.J. (2006) Hornblende dehydration reactions during magma ascent at Soufrière Hills Volcano, Montserrat. Contributions to Mineralogy and Petrology, 151(2), 121–140.
- Chazot, G., Menzies, M.A., and Harte, B. (1996) Determination of partition coefficients between apatite, clinopyroxene, amphibole, and melt in natural spinel lherzolites from Yemen: implications for wet melting of the lithospheric mantle. Geochimica et Cosmochimica Acta, 60(3), 423–437.
- Chazot, G., Charpentier, S., Kornprobst, J., Vannucci, R., and Luais, B. (2005) Lithospheric mantle evolution during continental break-up: The West Iberia non-volcanic passive margin. Journal of Petrology, 46(12), 2527–2568.
- Costa, F., and Chakraborty, S. (2004) Decadal time gaps between mafic intrusion and silicic eruption obtained from chemical zoning patterns in olivine. Earth and Planetary Science Letters, 227(3), 517–530.
- Costa, F., Scaillet, B., and Pichavant, M. (2004) Petrological and experimental constraints on the pre-eruption conditions of Holocene dacite from Volcán San Pedro (36°S, Chilean Andes) and the importance of sulphur in silicic subduction-related magmas. Journal of Petrology, 45(4), 855–881.
- Dalpé, C., and Baker, D.R. (2000) Experimental investigation of large-ion-lithophileelement-, high-field-strength-element- and rare-earth-element-partitioning between calcic amphibole and basaltic melt: The effects of pressure and oxygen fugacity. Contributions to Mineralogy and Petrology, 140(2), 233–250.
- Davidson, J., and Wilson, M. (2011) Differentiation and source processes at Mt Pelée and the Quill; Active volcanoes in the Lesser Antilles Arc. Journal of Petrology, 52(7-8), 1493–1531.
- Davidson, J., Turner, S., Handley, H., Macpherson, C., and Dosseto, A. (2007) Amphibole "sponge" in arc crust? Geology, 35(9), 787–790.
- Davidson, J., Turner, S., and Plank, T. (2013) Dy/Dy*: Variations arising from mantle sources and petrogenetic processes. Journal of Petrology, 54(3), 525–537.
- DeBari, S.M., and Coleman, R. (1989) Examination of the deep levels of an island arc: Evidence from the Tonsina Ultramafic-Mafic Assemblage, Tonsina, Alaska. Journal of Geophysical Research: Solid Earth, 94(B4), 4373–4391.
- Demény, A., Vennemann, T.W., Hegner, E., Ahijado, A., Casillas, R., Nagy, G., Homonnay, Z., Gutierrez, M., and Szabó, Cs. (2004) H, O, Sr, Nd, and Pb isotopic evidence for recycled oceanic crust in the Transitional Volcanic Group of Fuerteventura, Canary Islands, Spain. Chemical Geology, 205(1), 37–54.
- Dygert, N., Liang, Y., Sun, C., and Hess, P. (2014) An experimental study of trace element partitioning between augite and Fe-rich basalts. Geochimica et Cosmochimica Acta. 132. 170–186.
- Foden, J.D., and Green, D.H. (1992) Possible role of amphibole in the origin of andesite: some experimental and natural evidence. Contributions to Mineralogy and Petrology, 109(4), 479–493.
- Gaetani, G.A., and Grove, T.L. (1995) Partitioning of rare earth elements between clinopyroxene and silicate melt crystal-chemical controls. Geochimica et Cosmochimica Acta. 59(10), 1951–1962.
- Gardner, J.E., Rutherford, M., Carey, S., and Sigurdsson, H. (1995) Experimental constraints on pre-eruptive water contents and changing magma storage prior to explosive eruptions of Mount St. Helens volcano. Bulletin of Volcanology, 57(1), 1–17.
- Gourgaud, A., Fichaut, M., and Joron, J.L. (1989) Magmatology of Mt. Pelée (Martinique, FWI). I: Magma mixing and triggering of the 1902 and 1929 Pelean nuées ardentes. Journal of Volcanology and Geothermal Research, 38(1), 143–169.
- Green, T.H., and Pearson, N.J. (1985) Experimental determination of REE partition coefficients between amphibole and basaltic to andesitic liquids at high pressure. Geochimica et Cosmochimica Acta, 49(6), 1465–1468.
- Grégoire, M., Moine, B.N., O'Reilly, S.Y., Cottin, J.Y., and Giret, A. (2000) Trace element residence and partitioning in mantle xenoliths metasomatized by highly alkaline, silicate-and carbonate-rich melts (Kerguelen Islands, Indian Ocean). Journal of Petrology, 41(4), 477–509.
- Grove, T.L., Donnelly-Nolan, J.M., and Housh, T. (1997) Magmatic processes that generated the rhyolite of Glass Mountain, Medicine Lake volcano, N. California. Contributions to Mineralogy and Petrology, 127(3), 205–223.

- Grove, T.L., Elkins-Tanton, L.T., Parman, S.W., Chatterjee, N., Müntener, O., and Gaetani, G.A. (2003) Fractional crystallization and mantle-melting controls on calc-alkaline differentiation trends. Contributions to Mineralogy and Petrology, 145(5), 515–533.
- Grove, T.L., Baker, M.B., Price, R.C., Parman, S.W., Elkins-Tanton, L.T., Chatterjee, N., and Müntener, O. (2005) Magnesian andesite and dacite lavas from Mt. Shasta, northern California: products of fractional crystallization of H₂O-rich mantle melts. Contributions to Mineralogy and Petrology, 148(5), 542–565.
- Hawthorne, F.C. (1983) The crystal chemistry of the amphiboles. Canadian Mineralogist, 2(2), 173–480.
- Heliker, C. (1995) Inclusions in Mount St. Helens dacite erupted from 1980 through 1983. Journal of Volcanology and Geothermal Research, 66(1), 115–135.
- Hill, E., Wood, B.J., and Blundy, J.D. (2000) The effect of Ca-Tschermaks component on trace element partitioning between clinopyroxene and silicate melt. Lithos, 53(3), 203–215.
- Hilyard, M., Nielsen, R.L., Beard, J.S., Patinō-Douce, A., and Blencoe, J. (2000) Experimental determination of the partitioning behavior of rare earth and high field strength elements between pargasitic amphibole and natural silicate melts. Geochimica et Cosmochimica Acta, 64(6), 1103–1120.
- Holtz, F., Sato, H., Lewis, J., Behrens, H., and Nakada, S. (2004) Experimental petrology of the 1991–1995 Unzen Dacite, Japan. Part I: Phase relations, phase composition and pre-eruptive conditions. Journal of Petrology, 46(2), 319–337.
- Ionov, D.A., and Hofmann, A.W. (1995) Nb-Ta-rich mantle amphiboles and micas: Implications for subduction-related metasomatic trace element fractionations. Earth and Planetary Science Letters, 131(3), 341–356.
- Jagoutz, O.E., Burg, J.-P., Hussain, S., Dawood, H., Pettke, T., Iizuka, T., and Maruyama, S. (2009) Construction of the granitoid crust of an island arc part I: Geochronological and geochemical constraints from the plutonic Kohistan (NW Pakistan). Contributions to Mineralogy and Petrology, 158(6), 739–755.
- Kawamoto, T. (1996) Experimental constraints on differentiation and H₂O abundance of calc-alkaline magmas. Earth and Planetary Science Letters, 144(3-4), 577–589.
- Kelemen, P.B., Yogodzinski, G.M., and Scholl, D.W. (2003) Along-strike variation in the Aleutian Island Arc: Genesis of high Mg# andesite and implications for continental crust. In J. Eiler., Ed., Inside the Subduction Factory. Geophysical Monograph, American Geophysical Union 138, 223–276.
- Kelley, K.A., and Cottrell, E. (2009) Water and the oxidation state of subduction zone magmas. Science, 325, 605–607.
- Klein, M., Stosch, H.-G., and Seck, H.A. (1997) Partitioning of high field-strength and rare-earth elements between amphibole and quartz-dioritic to tonalitic melts: An experimental study. Chemical Geology, 138(3), 257–271.
- Lapierre, H., Ortiz, L.E., Abouchami, W., Monod, O., Coulon, C., and Zimmermann, J.-L. (1992) A crustal section of an intra-oceanic island are: The Late Jurassic-Early Cretaceous Guanajuato magmatic sequence, central Mexico. Earth and Planetary Science Letters, 108(1-3), 61–77.
- Larocque, J., and Canil, D. (2010) The role of amphibole in the evolution of arc magmas and crust: the case from the Jurassic Bonanza arc section, Vancouver Island, Canada. Contributions to Mineralogy and Petrology, 159(4), 475–492.
- LaTourrette, T., Hervig, R.L., and Holloway, J.R. (1995) Trace element partitioning between amphibole, phlogopite, and basanite melt. Earth and Planetary Science Letters, 135(1), 13–30.
- Leake, B.E., Woolley, A.R., Arps, C.E., Birch, W.D., Gilbert, C.M., Grice, J.D., Hawthorne, F.C., Kato, A., Kisch, H.J., Krivovichev, V.G., and others. (1997) Nomenclature of amphiboles: report of the subcommittee on amphiboles of the International Mineralogical Association, Commission on New Minerals and Mineral Names. Canadian Mineralogist, 35(1), 219–246.
- Lo Casio, M., Liang, Y., Shimizu, N., and Hess, P.C. (2008) An experimental study of the grain-scale processes of peridotite melting: Implications for major and trace element distribution during equilibrium and disequilibrium melting. Contributions to Mineralogy and Petrology, 156(1), 87–102.
- Lundstrom, C.C., Shaw, H.F., Ryerson, F.J., Williams, Q., and Gill, J. (1998) Crystal chemical control of clinopyroxene-melt partitioning in the Di-Ab-An system: Implications for elemental fractionations in the depleted mantle. Geochimica et Cosmochimica Acta, 62(16), 2849–2862.
- Martel, C., Pichavant, M., Bourdier, J.-L., Traineau, H., Holtz, F., and Scaillet, B. (1998) Magma storage conditions and control of eruption regime in silicic volcanoes: experimental evidence from Mt. Pelée. Earth and Planetary Science Letters, 156(1), 89–99.
- Martel, C., Pichavant, M., Holtz, F., Scaillet, B., Bourdier, J.-L., and Traineau, H. (1999) Effects of f_{0_2} and H_2O on andesite phase relations between 2 and 4 kbar. Journal of Geophysical Research: Solid Earth, 104(B12), 29,453–29,470.
- Mayer, B., Jung, S., Romer, R.L., Stracke, A., Haase, K.M., and Garbe-Schönberg, C.D. (2013) Petrogenesis of tertiary hornblende-bearing lavas in the Rhön, Germany. Journal of Petrology, 54(10), 2095–2123.
- McDonough, W.F., and Sun, S.S. (1995) The composition of the Earth. Chemical Geology, 120(3-4), 223–253.
- Médard, E., Schmidt, M.W., Schiano, P., and Ottolini, L. (2006) Melting of amphibolebearing wehrlites: An experimental study on the origin of ultra-calcic nephelinenormative melts. Journal of Petrology, 47(3), 481–504.
- Moine, B., Grégoire, M., O'Reilly, S.Y., Sheppard, S.M.F., and Cottin, J.Y. (2001) High field strength element fractionation in the upper mantle: Evidence from

- amphibole-rich composite mantle xenoliths from the Kerguelen Islands (Indian Ocean). Journal of Petrology, 42(11), 2145–2167.
- Moore, G., and Carmichael, I.S.E. (1998) The hydrous phase equilibria (to 3 kbar) of an andesite and basaltic andesite from western Mexico: Constraints on water content and conditions of phenocryst growth. Contributions to Mineralogy and Petrology, 130(3-4), 304–319.
- Mortazavi, M., and Sparks, R.S.J. (2004) Origin of rhyolite and rhyodacite lavas and associated mafic inclusions of Cape Akrotiri, Santorini: The role of wet basalt in generating calcalkaline silicic magmas. Contributions to Mineralogy and Petrology, 146(4), 397–413.
- Nandedkar, R.H. (2014) Evolution of hydrous mantle-derived cale-alkaline liquids by fractional crystallization at 0.7 and 0.4 GPa—An experimental study. Diss., Eidgenössische Technische Hochschule ETH Zürich, Nr. 21411.
- Nandedkar, R.H., Ulmer, P., and Müntener, O. (2014) Fractional crystallization of primitive, hydrous arc magmas: An experimental study at 0.7 GPa. Contributions to Mineralogy and Petrology, 167(6), 1015.
- Nandedkar, R.H., Hürlimann, N., Ulmer, P., and Müntener, O. (2016) Amphibole–melt trace element partitioning of fractionating calc-alkaline magmas in the lower crust: an experimental study. Contributions to Mineralogy and Petrology, 171(8-9), 71.
- Nekvasil, H., Dondolini, A., Horn, J., Filiberto, J., Long, H., and Lindsley, D.H. (2004) The origin and evolution of silica-saturated alkalic suites: An experimental study. Journal of Petrology, 45(4), 693–721.
- Neumann, E.-R., Wulff-Pedersen, E., Simonsen, S.L., Pearson, N.J., Martí, J., and Mitjavila, J. (1999) Evidence for fractional crystallization of periodically refilled magma chambers in Tenerife, Canary Islands. Journal of Petrology, 40(7), 1089–1123.
- Nicholls, I.A., and Harris, K.L. (1980) Experimental rare earth element partition coefficients for garnet, clinopyroxene and amphibole coexisting with andesitic and basaltic liquids. Geochimica et Cosmochimica Acta, 44(2), 287–308.
- Nye, C.J., and Turner, D.L. (1990) Petrology, geochemistry, and age of the Spurr volcanic complex, eastern Aleutian arc. Bulletin of Volcanology, 52(3), 205–226.
- Pallister, J.S., Hoblitt, R.P., Meeker, G.P., Knight, R.J., and Siems, D.F. (1996) Magma mixing at Mount Pinatubo: petrographic and chemical evidence from the 1991 deposits. In R.S. Punongbayan and C.G. Newhall, Eds., Fire and Mud: Eruptions and lahars of Mount Pinatubo, Philippines, p. 687–731. University of Washington Press, Seattle.
- Pallister, J.S., Thornber, C.R., Cashman, K.V., Clynne, M.A., Lowers, H.A., Mandeville, C.W., Brownfield, I.K., and Meeker, G.P. (2008) Petrology of the 2004-2006 Mount St. Helens lava dome-implications for magmatic plumbing and eruption triggering. U.S. Geological Survey Professional Paper 1750, 647–702.
- Parkinson, I.J., and Arculus, R.J. (1999) The redox state of subduction zones: Insights from arc-peridotites. Chemical Geology, 160(4), 409–423.
- Peters, S.T., Troll, V.R., Weis, F.A., Dallai, L., Chadwick, J.P., and Schulz, B. (2017) Amphibole megacrysts as a probe into the deep plumbing system of Merapi volcano, Central Java, Indonesia. Contributions to Mineralogy and Petrology, 172(4), 16.
- Pichavant, M., Martel, C., Bourdier, J.-L., and Scaillet, B. (2002) Physical conditions, structure, and dynamics of a zoned magma chamber: Mount Pelée (Martinique, Lesser Antilles Arc). Journal of Geophysical Research: Solid Earth, 107(B5), 2003
- Pilet, S., Baker, M.B., and Stolper, E.M. (2008) Metasomatized lithosphere and the origin of alkaline lavas. Science, 320, 916–919.
- Pilet, S., Ulmer, P., and Villiger, S. (2010) Liquid line of descent of a basanitic liquid at 1.5 GPa: Constraints on the formation of metasomatic veins. Contributions to Mineralogy and Petrology, 159(5), 621–643.
- Prouteau, G., and Scaillet, B. (2003) Experimental constraints on the origin of the 1991 Pinatubo dacite. Journal of Petrology, 44(12), 2203–2241.
- Putirka, K. (2016) Amphibole thermometers and barometers for igneous systems and some implications for eruption mechanisms of felsic magmas at arc volcanoes. American Mineralogist, 101, 841–858.
- Reubi, O., and Nicholls, I.A. (2004) Magmatic evolution at Batur volcanic field, Bali, Indonesia: Petrological evidence for polybaric fractional crystallization and implications for caldera-forming eruptions. Journal of Volcanology and Geothermal Research, 138(3), 345–369.
- Ridolfi, F., Puerini, M., Renzulli, A., Menna, M., and Toulkeridis, T. (2008) The magmatic feeding system of El Reventador volcano (Sub-Andean zone, Ecuador) constrained by texture, mineralogy and thermobarometry of the 2002 erupted products. Journal of Volcanology and Geothermal Research, 176(1), 94–106.
- Samaniego, P., Martin, H., Monzier, M., Robin, C., Fornari, M., Eissen, J.-P., and Cotten, J. (2005) Temporal evolution of magmatism in the Northern Volcanic Zone of the Andes: the geology and petrology of Cayambe Volcanic Complex (Ecuador). Journal of Petrology, 46(11), 2225–2252.
- Sato, H., Holtz, F., Behrens, H., Botcharnikov, R., and Nakada, S. (2005) Experimental petrology of the 1991–1995 Unzen dacite, Japan. Part II: Cl/OH partitioning between homblende and melt and its implications for the origin of oscillatory zoning of homblende phenocrysts. Journal of Petrology, 46(2), 339–354.
- Shane, P., Nairn, I.A., and Smith, V.C. (2005) Magma mingling in the ~50 ka Rotoiti eruption from Okataina Volcanic Centre: Implications for geochemical diversity and chronology of large volume rhyolites. Journal of Volcanology and Geothermal

- Research, 139(3), 295-313.
- Shannon, R.D. (1976) Revised effective ionic-radii and systematic studies of interatomic distances in halides and chalcogenides. Acta Crystallographica, A32, 751–767.
- Sisson, T.W. (1994) Hornblende-melt trace-element partitioning measured by ion microprobe. Chemical Geology, 117(1), 331–344.
- Smith, D.J. (2014) Clinopyroxene precursors to amphibole sponge in arc crust. Nature Communications, 5, 4329.
- Sorbadere, F., Schiano, P., and Métrich, N. (2013) Constraints on the origin of nepheline-normative primitive magmas in island arcs inferred from olivine-hosted melt inclusion compositions. Journal of Petrology, 54(2), 215–233.
- Spulber, S.D., and Rutherford, M.J. (1983) The origin of rhyolite and plagiogranite in oceanic crust: An experimental study. Journal of Petrology, 24(1), 1–25.
- Sun, C., and Liang, Y. (2012) Distribution of REE between clinopyroxene and basaltic melt along a mantle adiabat: Effects of major element composition, water, and temperature. Contributions to Mineralogy and Petrology, 163(5), 807–823.
- ——— (2013a) Distribution of REE and HFSE between low-Ca pyroxene and lunar picritic melts around multiple saturation points. Geochimica et Cosmochimica Acta. 119, 340–358.
- ——— (2013b) The importance of crystal chemistry on REE partitioning between mantle minerals (garnet, clinopyroxene, orthopyroxene, and olivine) and basaltic melts. Chemical Geology, 358, 23–36.
- Sun, C., Graff, M., and Liang, Y. (2017) Trace element partitioning between plagioclase and silicate melt: The importance of temperature and plagioclase composition, with implications for terrestrial and lunar magmatism. Geochimica et Cosmochimica Acta, 206, 273–295.
- Tappe, S., Foley, S.F., Stracke, A., Romer, R.L., Kjarsgaard, B.A., Heaman, L.M., and Joyce, N. (2007) Craton reactivation on the Labrador Sea margins: ⁴⁰Ar/⁵⁹Ar age and Sr-Nd-Hf-Pb isotope constraints from alkaline and carbonatite intrusives. Earth and Planetary Science Letters, 256(3), 433–454.
- Tiepolo, M., Vannucci, R., Bottazzi, P., Oberti, R., Zanetti, A., and Foley, S. (2000) Partitioning of rare earth elements, Y, Th, U, and Pb between pargasite, kaersuite, and basanite to trachyte melts: Implications for percolated and veined mantle. Geochemistry, Geophysics, Geosystems, 1(8), DOI: 10.1029/2000GC000064.
- Tiepolo, M., Oberti, R., Zanetti, A., Vannucci, R., and Foley, S.F. (2007) Trace-element partitioning between amphibole and silicate melt. Reviews in Mineralogy and Geochemistry, 67, 417–452.
- Toya, N., Ban, M., and Shinjo, R. (2005) Petrology of Aoso volcano, northeast Japan arc: temporal variation of the magma feeding system and nature of low-K amphibole andesite in the Aoso-Osore volcanic zone. Contributions to Mineralogy and Petrology. 148(5), 566–581.
- Vannucci, R., Piccardo, G.B., Rivalenti, G., Zanetti, A., Rampone, E., Ottolini, L., Oberti, R., Mazzucchelli, M., and Bottazzi, P. (1995) Origin of LREE-depleted amphiboles in the subcontinental mantle. Geochimica et Cosmochimica Acta, 59(9) 1763–1771
- Vaselli, O., Downes, H., Thirlwall, M., Dobosi, G., Coradossi, N., Seghedi, I., Szakacs, A., and Vannucci, R. (1995) Ultramafic xenoliths in Plio-Pleistocene alkali basalts from the Eastern Transylvanian Basin: Depleted mantle enriched by vein metasomatism. Journal of Petrology, 36(1), 23–53.
- Wade, J.A., Plank, T., Stern, R.J., Tollstrup, D.L., Gill, J.B., O'Leary, J.C., Eiler, J.M., Moore, R.B., Woodhead, J.D., Trusdell, F., Fischer, T.P., and Hilton, D.R. (2005) The May 2003 eruption of Anatahan volcano, Mariana Islands: Geochemical evolution of a silicic island-arc volcano. Journal of Volcanology and Geothermal Research, 146(1), 139–170.
- Witt-Eickschen, G., Seck, H.A., Mezger, K., Eggins, S.M., and Altherr, R. (2003) Lithospheric mantle evolution beneath the Eifel (Germany): constraints from Sr– Nd–Pb isotopes and trace element abundances in spinel peridotite and pyroxenite xenoliths. Journal of Petrology, 44(6), 1077–1095.
- Wood, B.J., and Blundy, J.D. (1997) A predictive model for rare earth element partitioning between clinopyroxene and anhydrous silicate melt. Contributions to Mineralogy and Petrology, 129(2-3), 166–181.
- Wulff-Pedersen, E., Neumann, E.-R., and Jensen, B.B. (1996) The upper mantle under La Palma, Canary Islands: Formation of Si-K-Na-rich melt and its importance as a metasomatic agent. Contributions to Mineralogy and Petrology, 125(2-3), 113–139.
- Yao, L., Sun, C., and Liang, Y. (2012) A parameterized model for REE distribution between low-Ca pyroxene and basaltic melts with applications to REE partitioning in low-Ca pyroxene along a mantle adiabat and during pyroxenite-derived melt and peridotite interaction. Contributions to Mineralogy and Petrology, 164(2), 261–280.
- Zanetti, A., Vannucci, R., Bottazzi, P., Oberti, R., and Ottolini, L. (1996) Infiltration metasomatism at Lherz as monitored by systematic ion-microprobe investigations close to a hornblendite vein. Chemical Geology, 134(1), 113–133.

MANUSCRIPT RECEIVED FEBRUARY 17, 2017 MANUSCRIPT ACCEPTED JULY 7, 2017 MANUSCRIPT HANDLED BY CALVIN BARNES